International Journal of Thermofluids 22 (2024) 100648

Contents lists available at ScienceDirect

International Journal of Thermofluids

journal homepage: www.elsevier.com/locate/ijtf

Thermodynamics of variable thermophysical properties of non-Newtonian fluids with the exploration of antiviral and antibacterial mechanisms using silver nanoparticles

Ogiboina Ramakrishna [a,*], Bidemi Olumide Falodun [b], Oluwadamilare Joseph Akinremi [c,d,**], Ezekiel Olaoluwa Omole [c,d], Ahmed Senior Ismail [e], Femi Emmanuel Amoyedo [c,d]

[a] Department of Mathematics, Anurag University, Hyderabad Telangana, India
[b] Department of Mathematics and Computer Science, Elizade University, Ilara-Mokin, Ondo State, Nigeria
[c] Department of Physical Sciences (Mathematics Programme), Landmark University, Omu-Aran, Nigeria
[d] SDG 4: Quality Education Research Group, Landmark University, Omu-Aran, Nigeria
[e] Department of Integrated Applied Mathematics, University of New Hampshire, USA

ARTICLE INFO

Keywords:
Cattaneo-Christov theories
Spectral relaxation method
Gyrotactic microorganism
Casson-Walters-B fluids

ABSTRACT

This research is aimed at examining the thermodynamics of variable thermophysical properties of non-Newtonian fluids with the exploration of antiviral and antibacterial mechanisms. The mechanism of antiviral together with antibacterial was separately considered by utilizing the silver nanoparticles. The physical phenomenon comprising thermal radiation, magnetic field, chemical reaction, heat generation parameters, etc are presented as partial differential equations (PDEs). The formulated PDEs are changed into ordinary differential equations using suitable similarity variables. The spectral relaxation method (SRM) was employed to numerically solve the set of equations. The SRM is an iterative method that employs the basic techniques of the Gauss–Seidel approach. In addition, an experimental finding on the use of silver nanoparticles was conducted and the silver nanoparticles were found to be a good antimicrobial in dentistry. The magnetic field affects the size of silver nanoparticles within the boundary layer. This leads to a reduction in the replication of both viruses and bacteria within the boundary layer. In addition, the magnetic field was observed to shrink the non-Newtonian fluids by reducing the skin friction coefficient. In the analysis, a blockage to viral replication was noticed due to higher thermal radiation which increases the temperature. The magnetic parameter was observed to reduce infection by playing a significant role on the mechanisms of antiviral and antibacterial within the boundary layer.

1. Introduction

A non-Newtonian fluid is a type of fluid which do not follow Newton's viscosity law. It finds applications in numerous fields of engineering, especially in fluid mechanics. In modeling non-Newtonian fluids, the shear stress does not have a linear relationship with the shear rate. The non-Newtonian model is applicable in fields of sciences and engineering such as cosmetics, food processing, and biomedical engineering. Examples of non-Newtonian fluids are custard, toothpaste, ketchup, etc. The interest of many researchers in non-Newtonian fluid grows every day due to its numerous applications in our daily activities. Gbadeyan and Akinremi [1] studied entropy analysis of the nonlinear convective flow of Jeffrey non-Newtonian fluid by varying electrical and thermal conductivity. Vishalakshi et al. [2] explored the effect of MHD on the dynamics of non-Newtonian fluid flow past a penetrable stretching sheet. Idowu and Falodun [3] studied the flow behavior of non-Newtonian fluid by varying the thermal conductivity and viscosity. Algehyne et al. [4] studied the dynamics of non-Newtonian fluid by explaining the mechanical characteristics of MHD Maxwell fluid in a bi-directional convectively heated surface. The heated convective and magneto radiative boundary layer flow of non-Newtonian fluid across a penetrable inclined vertical plate was discussed by Sudarmozhi et al. [5]. Soliman [6] studied the MHD flow of non-Newtonian fluid of third grade through a penetrable medium and constant heat source.

* Corresponding author.
** Corresponding author at: Department of Physical Sciences (Mathematics Programme), Landmark University, Omu-Aran, Nigeria.
E-mail addresses: ramakrishna.maths@anurag.edu.in (O. Ramakrishna), falodunbidemi2014@gmail.com (B.O. Falodun), akinremi.joseph@lmu.edu.ng (O.J. Akinremi).

https://doi.org/10.1016/j.ijft.2024.100648
Received 29 January 2024; Received in revised form 29 March 2024; Accepted 31 March 2024
Available online 6 April 2024

Nomenclature

K_0	Coefficient of short memory
μ_0	Dynamic viscosity (kg/ms)
d	Tensor deformation rate
d^{∇}	Derivative of a tensor upper-convected
P_y	Fluid yield stress
ρ	Density of fluid (kg/m^3)
β	Casson parameter
p	Fluid pressure (Pa)
I	Identity tensor
v	Velocity vector (m/s)
∇	Gradient operator
η_0	Limiting viscosity at small rate
σ_s	Stefan-Boltzmann constant
k_e	Coefficient of mean absorption
$C_1, C_2, C_3, C_m, C_s, C_t$	Thermophoretic constant
λ_g	Fluid thermal conductivities
K_n	Knudsen number
N	Collocation number
u	Velocity in x-direction (m/s)
v	Velocity in y-direction (m/s)
σ	Electrical conductivity
B_0	Strength of magnetic field
k_p	Porosity coefficient
g	Gravity
β_1	Thermal expansion volumetric coefficient (K^{-1})
β_2	Concentration expansion volumetric coefficient (m^3/k mol)
C	Concentration of fluids (m^2 s^{-1})
C_∞	Concentration at free stream (mol)
β_3	Volumetric coefficient of density microorganisms expansion
T	Temperature of fluids (K)
T_∞	Temperature at free stream (K)
$k(T)$	Temperature dependent thermal conductivity (m^2/s)
c_p	Specific heat when pressure is constant (J/kg K)
q_r	Heat flux (W/m^2)
$\mu_b(T)$	Temperature-dependent dynamic viscosity (kg/ms)
Q_0	Coefficient of heat generation
D	Mass diffusivity (m^2 s^{-1})
k_T	Thermal diffusion ratio
c_s	Concentration susceptibility (k mol m^{-3})
τ	Nanoparticles coefficient
D_B	Brownian motion coefficient
β_i	Heat flux coefficient
$D(T)$	Temperature-dependent mass diffusivity
k_l	Coefficient of chemical reaction (k mol m^{-3})
V_T	Velocity of thermophoretic
T_m	Mean of fluids temperature (K)
β_j	Mass flux coefficient
$D_n(T)$	Temperature-dependent density microorganisms mass diffusivity
B	Constant
T_w	Wall temperature (K)
C_w	Wall concentration (mol)
N	Density microorganism of fluids

The study of hybrid nanofluids alongside ternary hybrid nanofluids contains metallic or polymer-based nano-sized powders combined with the normal fluid. This study finds applications in heat channels, solar energy, heat transmission, and coolant in equipment. The ternary hybrid nanoparticles are selected based on the thermophysical and rheological properties. Based on these various applications, Raza et al. [7] studied the role of nanolayer on the thermodynamics of trihybrid nanofluid via two porous disks. The significance of PHF and PST heating constraints on swirl flow of Al + Mg + $Ti0_2$ was investigated by Salah et al. [8] in a rotating cone. Sajjan et al. [9] elucidated nonlinear Boussinesq and Rosseland approximations on 3D dynamics through an interruption of ternary nanoparticles. Khan et al. [10] examined energy and mass transport of hybrid nanofluid dynamics within an extended cylinder with a magnetic dipole. Mixed convection nanofluid flow with heat source as well as chemical reaction through an inclined irregular surface was considered by Haq et al. [11]. Gladys and Reddy [12] studied non-Newtonian dynamics of nanofluids by varying viscosity and thermal conductivity. The study of Gurrampatic and Vijaya [13] examined the Buongiomo model with Brownian and thermophoretic diffusion for MHD Casson nanofluid.

In recent times, the significance of fluid flow due to gyrotactic microorganisms has been studied. Many authors have discussed heat and mass transmission in the dynamics of gyrotactic microorganisms. The nanofluids with microbe's existence are useful in many microsystems in determining cellulose and toxicity optimization. Ahmad et al. [14] studied the impact of swimming gyrotactic microorganisms alongside viscous dissipation on nanoparticle dynamics. The dynamics of nanoparticles in blood and the swimming of motile gyrotactic microorganisms through anisotropically tapered arteries have been investigated by Bhatti et al. [15]. Muhammad et al. [16] discussed the interaction of motile gyrotactic microorganisms with nanoparticles in an MHD Darcy-Forchheimer flow. Bhatti et al. [17] studied activation energy on the dynamics of gyrotactic microorganisms in magnetized nanofluids in a penetrable plate. Xu et al. [18] studied gyrotactic microorganism dynamics of Maxwell nanofluid within two parallel plates. Kada et al. [19] studied the significance of gyrotactic microorganisms and bioconvection radiative analysis with ferromagnetic nanoparticles. Chandra and Das [20] studied the impact of gyrotactic microorganisms in nanofluid through a penetrable medium towards an inclined stretching plate. Reddy and Sreedevi [21] studied unsteady gyrotactic microorganisms alongside magnetic nanofluid mass and heat transmission analysis in a chamber with thermal radiation.

The presence of microbes such as fungi, viruses, parasites, bacteria, and protozoa causes infectious diseases to human health. Infectious diseases have posed a burden to the economic and public health of the world in recent times. Antibiotic resistance takes place when bacteria escape the impact of antibiotics through different mechanisms. The abuse of drugs and the strong resistance that grown microbes possess to these antibiotics have limited the progress of the treatment. Hussain et al. [22] conducted a comprehensive review of nano-antivirals as agents against microorganisms. Franco et al. [23] examined metal-based nanoparticles, biomedical applications, and antibacterial mechanisms by considering the physico-chemical properties of nanoparticles. A mechanism of action on silver nanoparticles' potential for antiviral and antibacterial applications was investigated by Salleh et al. [24]. The recent research of Soares et al. [25] investigated prevalence alongside non-carious cervical lesions severity and dentin hypersensitivity. Brandelli [26] studied the interaction of nanostructure antimicrobials

with biological systems. Slaving et al. [27] studied the concept behind the mechanisms of antibacterial activity of metal nanoparticles.

A magnetic field describes the magnetic influence involved in a moving electric current, magnetic materials, and electric charges. The physical phenomenon takes place in magnetohydrodynamic majorly when a conductor moves into a magnetic field and electric current is hereby induced to form its magnetic field. The study of MHD has gained interest in recent times because of its technological and industrial applications in crystal growth, power generators, electromagnetic pumps, MHD accelerators, and reactor cooling. Idowu and Falodun [28] studied mechanisms of Soret–Dufour on MHD heat and mass transmission of Walters-B viscoelastic fluid. Gupta and Rana [29] conducted a comparative study on Rosseland's heat flux on 3D MHD stagnation point multiple slip dynamics. Wang et al. [30] examined non-Darcian dynamics of radiative ternary hybridity MHD dynamics. The analysis of electromagnetic trihybrid Ellis nanofluid dynamics influenced by a magnetic dipole together with chemical reaction was investigated by Rooman et al. [31]. Alhowaity et al. [32] studied non-Fourier energy transmission in power-law hybrid nanofluid dynamics past a moving sheet. An irreversibility analysis of electromagnetic hybrid nanofluid for heat flux Cattaneo-Christov was investigated by Qureshi [33]. Ullah et al. [34] studied Darcy-Forchheimer hybrid nanofluids dynamics with quadratic convection past a stretched tube. Adeyefa et al. [35] studied the numerical solution of second-order nonlinear partial differential equations originating from the physical phenomenon. Fadugba et al. [36] studied the development and analysis of a new third-order method for solving initial value problems. Li et al. [37] recently examined heat and mass transmission of Al2O3/H2O along with (Al2O3+Ag)/H2O nanofluids. Li et al. [38] explored generalized Lie similarity transformations for unsteady heat transfer flow by considering the impact of thermal radiation as well as internal heating. Effectiveness of melting phenomenon in double phase dusty carbon nanotubes Eyring–Powell fluid flow using heat transfer analysis has been considered by Li et al. [39]. Li et al. [40] explored applications of Soret and Dufour mechanisms for Maxwell nanomaterial by convectively heated surface.

This research conducted the thermodynamics of non-Newtonian fluids alongside the antibacterial and antiviral mechanisms using silver nanoparticles. The assessment of antibacterial mechanism was done using broth dilution while assessments of antiviral mechanisms were done by employing virus plaque assay. To the best of our knowledge, no study in literature has conducted research of this type. The present research work is very unique because the synthesis of silver nanoparticles and their interaction with non-Newtonian fluids has been extensively discussed. In addition, the significance of thermal radiation and magnetic field on viral replication as well as its infection has been discussed. To properly explain the physics of the problem, numerical simulations and an experimental assessment of antibacterial and antiviral mechanisms were explored in this study. This study finds usefulness in the health sector. The research is applicable in dentistry, cancer treatment, drug delivery, DNA analysis, biosensors, catalysis, and magnetic resonance imaging (MRI).

2. Mathematical modeling

Consider a steady, two-dimensional, incompressible laminar flow of non-Newtonian fluids through a penetrable stretching surface. The flow mechanisms was analyzed with both antiviral and antibacterial mechanisms by using the silver nanoparticles. The non-Newtonian fluids (Casson and Walters-B fluids) are considered by varying the thermophysical properties such as viscosity and thermal conductivity. Fungi and bacterial are considered as gyrotactic microorganisms in this research. To eradicate the infectious diseases that fungi and bacteria can cause, the silver nanoparticles alongside honey was employed as the antiviral and antibacterial agents. A nonlinear buoyancy effect alongside Joule heating are considered to be significant in this research.

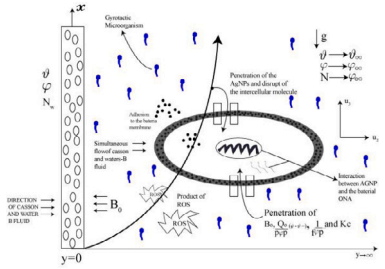

Fig. 1. Physical geometry for AgNps antibacteria mechanism.

The stretchable surface where the mechanisms of antiviral and antibacterial takes place are assumed to be porous while the gyrotactic microorganism swims within the boundary layer (see Figs. 1 and 2). At the stretched wall, the temperature (T_w), motile density concentration (N_w), and concentration (C_w) are considered to be significant. The temperature, concentration and motile density concentration at the free stream are T_∞ C_∞, and N_∞ respectively. A magnetic field of uniform strength was imposed transversely to the flow while the induced magnetic field are ignored because of a small Reynolds number. The thermal radiation, heat generation and Fourier heat flux are considered significant to explain the fluid thermal enhancement. The replication of the viruses and bacterial within the boundary layer as a result of magnetic field within the boundary layer leads to the inactivation of the pathogenic viruses and hereby magnetized both the viruses and bacterial. It has a practical applications on the use of electromagnetic waves to aid inactivate pathogenic virus. This is done by rapidly and homogeneously increases the generation of heat within the boundary layer. In addition, a magnetized viruses has a great attack on the bacterial within the boundary layer. Hence, a magnetotactic bacterial hereby aligned with the magnetic field imposed to the boundary layer.

2.1. Antibacterial mechanism of AgNPs

The silver nanoparticles penetrate the bacteria cell through the porous medium and change the cell membrane structure which leads to the death of the cell. The permeability of cell membranes hereby increases and gives rise to reactive oxygen species which disturb the deoxyribonucleic acid replications in dentistry. For acrylic resins for removal of dentures in prosthetic treatment. The antibacterial mechanism of silver nanoparticles disrupts the cytoplasmic membrane and cell wall. It also perforates the membrane.

2.2. Antiviral mechanism of AgNPs

The silver nanoparticles play a vital role in the antiviral mechanism. It served as an antiviral drug for viruses such as hepatitis B virus, monkeypox virus, human immunodeficiency virus, respiratory syntactical virus, and herpes simple virus. The mechanism of antiviral in this research is basically on the viruses encountered by humans due to changes in environment and host. The virus replication as explained in Fig. 2 is due to virus adsorption, virus penetration, genome replication, and protein synthesis. The silver nanoparticles is applied in dentistry for disinfection and prevention of infections in the oral cavity. The AgNPs is a metallic nanoparticles which has the implications of eliminating fungal and bacterial infections in the mouth. AgNPs also helps in removing tartar and plaque. In dentistry, an adhesives and composite resins together with AgNPs is employed to minimize tooth loss and biofilm. A very high intensity of magnetic field into the skin friction as an antimicrobial agents greatly affects the movement of charged particles through the atomic nucleic and hereby acts to slow down the

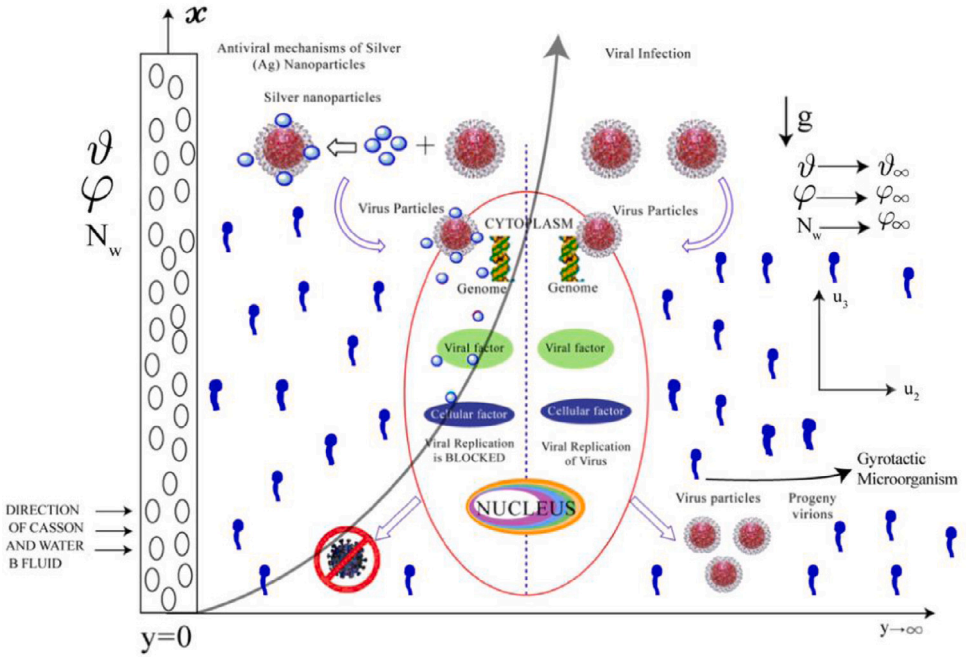

Fig. 2. Physical geometry for AgNps antiviral mechanism.

coefficient of skin friction. Due to the assumptions above, the physical model are given as follows (see Idowu and Falodun [30]):

$$\frac{\partial u_2}{\partial x}+\frac{\partial u_3}{\partial y}=0 \tag{1}$$

$$u_2\frac{\partial u_2}{\partial x}+u_3\frac{\partial u_2}{\partial y}=\frac{\partial \tau_{xx}}{\partial x}+\frac{\partial \tau_{xy}}{\partial y}-\frac{\sigma B_0^2}{\rho}u_2-\frac{\mu_b}{k_p}u_2 + g\beta_1(\vartheta-\vartheta_\infty)+g\beta_2(\varphi-\varphi_\infty)+g\beta_3(N-N_\infty) \tag{2}$$

$$u_2\frac{\partial \vartheta}{\partial x}+u_3\frac{\partial \vartheta}{\partial y}=\frac{k(\vartheta)}{\rho c_p}\frac{\partial^2\vartheta}{\partial y^2}+\frac{k(\vartheta)}{\rho c_p}\frac{\partial \vartheta}{\partial y}\frac{\partial k(\vartheta)}{\partial y}-\frac{1}{\rho c_p}\frac{\partial q_r}{\partial y} + \frac{\mu_b(\vartheta)}{\rho c_p}\left(1+\frac{1}{\beta}\right)\frac{\partial}{\partial y}\left(\mu\left(\frac{\partial u_2}{\partial y}\right)^2\right)+\frac{Q_0}{\rho c_p}(\vartheta-\vartheta_\infty) + \frac{Dk_\vartheta}{c_s c_p}\frac{\partial^2\varphi}{\partial y^2}+\tau\left[D_B\frac{\partial \varphi}{\partial y}\frac{\partial \vartheta}{\partial y}+\frac{D_\vartheta}{\vartheta_\infty}\left(\frac{\partial \vartheta}{\partial y}\right)^2\right] - \beta_i\left[u_2\frac{\partial u_2}{\partial x}\frac{\partial \vartheta}{\partial x}+u_3\frac{\partial u_3}{\partial y}\frac{\partial \vartheta}{\partial y}+u_2\frac{\partial u_3}{\partial x}\frac{\partial \vartheta}{\partial y}+u_3\frac{\partial u_2}{\partial y}\frac{\partial \vartheta}{\partial x} +2u_2u_3\frac{\partial^2\vartheta}{\partial x\partial y}+u_2^2\frac{\partial^2\vartheta}{\partial x^2}+u_3^2\frac{\partial^2\vartheta}{\partial y^2}\right] \tag{3}$$

$$u_2\frac{\partial \varphi}{\partial x}+u_3\frac{\partial \varphi}{\partial y}=D(\vartheta)\frac{\partial^2\varphi}{\partial y^2}-k_l(\varphi-\varphi_\infty)-\frac{\partial(V_\vartheta\varphi)}{\partial y}+\frac{Dk_\vartheta}{\vartheta_m}\frac{\partial^2\vartheta}{\partial y^2}+\frac{D_\vartheta}{\vartheta_\infty}\frac{\partial^2\vartheta}{\partial y^2} - \beta_j\left[u_2\frac{\partial u_2}{\partial x}\frac{\partial \varphi}{\partial x}+u_3\frac{\partial u_3}{\partial y}\frac{\partial \varphi}{\partial y}+u_2\frac{\partial u_3}{\partial x}\frac{\partial \varphi}{\partial y}+u_3\frac{\partial u_2}{\partial y}\frac{\partial \varphi}{\partial x} +2u_2u_3\frac{\partial^2\varphi}{\partial x\partial y}+u_2^2\frac{\partial^2\varphi}{\partial x^2}+u_3^2\frac{\partial^2\varphi}{\partial y^2}\right] \tag{4}$$

$$u_2\frac{\partial N}{\partial x}+u_3\frac{\partial N}{\partial y}=D_n(\vartheta)\frac{\partial^2 N}{\partial y^2}-\frac{bWc}{\Delta\varphi}\left[\frac{\partial N}{\partial y}\frac{\partial \varphi}{\partial y}+\frac{\partial^2\varphi}{\partial y^2}\right] \tag{5}$$

subject to the boundary conditions:

$$u_2=Bx\ ,u_3=-v(x)\ ,\vartheta=\vartheta_w\ ,\varphi=\varphi_w\ \ ,at\ \ y=0 \tag{6}$$

$$u_2\longrightarrow 0\ ,\varphi\longrightarrow\varphi_\infty\ ,\varphi\longrightarrow\varphi_\infty\ \ ,as\ \ y\longrightarrow\infty \tag{7}$$

3. Experimental study

3.1. Assessment of antibacterial mechanism

The broth dilution or minimum inhibition concentration (MIC) is employed in this study as antimicrobial criteria to investigate the antimicrobial compounds. This research employed the broth dilution method to know the required concentration of polymers to deactivate the bacteria present in non-Newtonian fluids such as concentrated fruit consumed by humans, the developed antimicrobial agents are employed as an antibiotic for the treatment. However, the polymer solution possesses a concentration of about 500 to 1.75 ppm. The MIC is explained in this research to impede the growth of bacteria in non-Newtonian fluids. In addition, the MIC method was used in this research to stop the replication of bacteria from the wall of the vertical surface to the boundary layer. All fluid properties are found to be insignificant outside the boundary layer, that is, at the free stream. The imposed magnetic field finds applications in viral diagnostics for a very rapid viral detection. Also, a magnetic hyperthermia is useful in generating a localized heat. The heat generated by this magnetic hyperthermia due to the presence of heat generation parameter hereby destroy all the virus-infected cells. In addition, the magnetic field enhances blood flow and helps the immune agents as well as the cells to act faster.

3.2. Assessment of antiviral mechanisms

The virus plaque assay was utilized on the cells within the boundary layer to stop its replication. The antiviral activity was hereby evaluated to a very low concentration level. The thermal expansion and the heat generated by the radiative heat flux and the heat generation coefficient kill this virus on the non-Newtonian fluids. Hence, the concentration of the virus is drastically reduced on the boundary. In addition, honey has been employed in this research as an antiviral means of deactivating the activities of viruses within the boundary layer. Therefore, the virucidal efficiency reduces drastically. where M and N as plagues numbers detected from the control

In Eq. (2), the Cauchy stress function was applied in x-y-momentum while τ_{xx}, τ_{xy} are stress matrix function. Based on the previous study of

Tonekaboni et al. [41], the Walters-B stress matrix function in the form:

$$\tau = 2\tau_0 d - 2k_0 d^{\nabla} \tag{8}$$

The Eq. (8) above indicates the Walters-B equation. The simultaneous flow of Casson along with Walters-B fluid is explored in this paper. Hence, the analysis involved double fluids parameters. Fredrickson [42] defined viscosity as $\left(\tau = \mu \frac{\partial u_2}{\partial y} \mid_y = 0\right)$ and explained Casson fluid rheological equation as:

$$\tau_{ij} = \left(\mu_b(\vartheta) + \frac{P_y}{\sqrt{2\pi}}\right) 2e_{ij} \quad for \quad \pi > \pi_c$$

$$\tau_{ij} = \left(\mu_b(\vartheta) + \frac{P_y}{\sqrt{2\pi_c}}\right) 2e_{ij} \quad for \quad \pi < \pi_c \tag{9}$$

where

$$P_y = \frac{\mu_b(\vartheta)\sqrt{(2\pi)}}{\beta} \tag{10}$$

From the above, $\pi = e_{ij}e_{ij}$ means that rate of deformation components multiplying itself, π_c means Casson model critical value. In a scenario where $\pi > \pi_c$, it means that:

$$\mu_0 = \mu_b(\vartheta) + \frac{P_y}{\sqrt{2\pi}} \tag{11}$$

Simplifying Eq. (8) by putting it to (9), the dynamic viscosity leads to:

$$\mu_0 = \frac{\mu_b(\vartheta)}{\rho}\left(1 + \frac{1}{\beta}\right) \tag{12}$$

Based on Mehmood et al. [43], Walters-B Cauchy stress tensor (S) is defined in the form:

$$S = -p\vartheta + \tau \tag{13}$$

$$\tau = 2\eta_0 e - 2k_0 \frac{\delta e}{\delta t} \tag{14}$$

Also, rate of strain tensor (e) is given by:

$$2e = \nabla(v) + \nabla(v)^T \tag{15}$$

The convected differentiation of strain tensor rate is given by:

$$\frac{\delta(e)}{\delta t} = \frac{\partial(e)}{\partial t} + v.\nabla(e) - e.\nabla(v) - (\nabla(v))^T.e \tag{16}$$

where η_0 and k_0 are defined as:

$$\eta_0 = \int_0^{\infty} \lambda(\xi) d\xi \tag{17}$$

$$k_0 = \int_0^{\infty} \tau\lambda(\xi) d\xi \tag{18}$$

where Walters [44] explained $\lambda(\xi)$ as the relaxation spectrum. All the above explanations are the mathematical model for Walters-B fluid by considering that it is very short such that $\int_0^{\infty} \tau^n \lambda(\tau) d\tau, \quad n \geq 2$ are ignored. Taking into consideration Eqs. (11)–(16) relations, the stress components leads to:

$$\tau = \begin{bmatrix} \tau_{xx} & \tau_{xy} \\ \tau_{yx} & \tau_{yy} \end{bmatrix} \tag{19}$$

$$\tau_{xx} = 2\mu_0 \frac{\partial u_2}{\partial x} - 2k_0 \times \left[u_2 \frac{\partial^2 u_2}{\partial x^2} + u_3 \frac{\partial^2 u_2}{\partial x \partial y} - 2\left(\left(\frac{\partial u_2}{\partial x}\right)^2 + \frac{1}{2}\frac{\partial u_2}{\partial y}\left(\frac{\partial u_2}{\partial y} + \frac{\partial u_3}{\partial x}\right)\right)\right] \tag{20}$$

$$\tau_{yx} = \tau_{xy} = \mu_0\left(\frac{\partial u_2}{\partial y} + \frac{\partial u_3}{\partial x}\right) - 2k_0\left[\frac{1}{2}u_2\left(\frac{\partial^2 u_3}{\partial x^2} + \frac{\partial^2 u_2}{\partial x \partial y}\right) + \frac{1}{2}u_3\left(\left(\frac{\partial^2 u_2}{\partial y^2} + \frac{\partial^2 u_3}{\partial x \partial y}\right) - \left(\frac{\partial u_2}{\partial x}\frac{\partial u_3}{\partial x} + \frac{\partial u_2}{\partial y}\frac{\partial u_3}{\partial y}\right)\right)\right] \tag{21}$$

$$\tau_{yy} = 2\mu_0 \frac{\partial u_3}{\partial y} - 2k_0\left[\frac{\partial^2 u_3}{\partial t \partial x} + u_2 \frac{\partial u_3}{\partial x \partial y} + u_3 \frac{\partial^2 u_3}{\partial y^2} - 2\left(\frac{1}{2}\frac{\partial u_3}{\partial x}\left(\frac{\partial u_2}{\partial y} + \frac{\partial u_3}{\partial x}\right) + \left(\frac{\partial u_3}{\partial y}\right)^2\right)\right] \tag{22}$$

where $\tau_{xx}, \tau_{xy}, \tau_{yx}$ and τ_{yy} are stress matrix components. Applying differentiation on the above stress tensor to obtain:

$$\rho\left(\frac{\partial \tau_{xx}}{\partial x} + \frac{\partial \tau_{xy}}{\partial y}\right) = \mu_0\left(\frac{\partial^2 u_2}{\partial y^2}\right) - k_0\left(u_3 \frac{\partial^3 u_2}{\partial y^3} + u_2 \frac{\partial^3 u_2}{\partial x \partial y^2} - 2\frac{\partial u_2}{\partial y}\frac{\partial^2 u_2}{\partial x \partial y} - 3\frac{\partial u_2}{\partial x}\frac{\partial^2 u_2}{\partial y^2}\right) \tag{23}$$

By considering the heat flux q_r is simplified by utilizing the Rosseland diffusion approximation as explained in Alao et al. [45] and Fagbade et al. [46] such that:

$$q_r = -\frac{4\sigma_s}{3k_e}\frac{\partial \vartheta^4}{\partial y} \tag{24}$$

Considering that the differences in temperature on the flow regime is very small such that ϑ^4 is simplified in a linear form about ϑ_∞ utilizing Taylor series and ignore terms of higher order to obtain:

$$\vartheta^4 \approxeq 4\vartheta_\infty^3 \vartheta - 3\vartheta_\infty^4 \tag{25}$$

Utilizing Eq. (24) on (23) and implement on the third term of Eq. (3) to obtain:

$$-\frac{\partial q_r}{\partial y} = \frac{16\sigma_s \vartheta_\infty^3}{3k_e}\frac{\partial^2 \vartheta}{\partial y^2} \tag{26}$$

By exploring thermophoresis in this paper, V_ϑ is the velocity of thermophoretic, and k is the coefficient of thermophoretic which are defined as:

$$V_\vartheta = -k\nu\frac{\nabla\vartheta}{\vartheta_{ref}} = -\frac{k\nu}{\vartheta_{ref}}\frac{\partial \vartheta}{\partial y} \tag{27}$$

$$k = \frac{2C_s\left(\frac{\lambda_g}{\lambda_p} + C_t K_n\right)\left[1 + K_n\left(C_1 + C_2 e^{\frac{-C_3}{K_n}}\right)\right]}{\left(1 + 3C_m K_n\right)\left(1 + 2\frac{\lambda_g}{\lambda_p} + 2C_t K_n\right)} \tag{28}$$

Based on the above simplifications on Casson-Walters-B fluids and utilizing equations (10), (22), (24), and (25) on the flow Eqs. (1)–(4) leads to:

$$\frac{\partial u_2}{\partial x} + \frac{\partial u_3}{\partial y} = 0 \tag{29}$$

$$u_2\frac{\partial u_2}{\partial x} + u_3\frac{\partial u_2}{\partial y} = \frac{\mu_b(\vartheta)}{\rho}\left(1 + \frac{1}{\beta}\right)\frac{\partial^2 u_2}{\partial y^2} + \frac{1}{\rho}\left(1 + \frac{1}{\beta}\right)\frac{\partial u_2}{\partial y}\frac{\partial \mu_b(\vartheta)}{\partial \vartheta}\frac{\partial \vartheta}{\partial y} - \frac{\sigma B_0^2}{\rho}u_2 - \frac{\mu_b}{k_p}\left(1 + \frac{1}{\beta}\right)u_2 - \frac{K_0}{\rho}\left(u_3\frac{\partial^3 u_2}{\partial y^3} + u_2\frac{\partial^3 u_2}{\partial x \partial y^2} - 2\frac{\partial u_2}{\partial y}\frac{\partial^2 u_2}{\partial x \partial y} - 3\frac{\partial u_2}{\partial x}\frac{\partial^2 u_2}{\partial y^2}\right) + g\beta_1(\vartheta - \vartheta_\infty) + g\beta_2(\varphi - \varphi_\infty) + g\beta_3(N - N_\infty) \tag{30}$$

$$u_2\frac{\partial \vartheta}{\partial x} + u_3\frac{\partial \vartheta}{\partial y} = D_n\frac{\partial^2 N}{\partial y^2} + D_n\frac{\partial N}{\partial y}\frac{\partial D_n(\vartheta)}{\partial y} - \frac{1}{\rho c_p}\frac{\partial q_r}{\partial y} + \frac{\mu_b(\vartheta)}{\rho c_p}\left(1 + \frac{1}{\beta}\right)\frac{\partial}{\partial y}\left(\mu\left(\frac{\partial u_2}{\partial y}\right)^2\right) + \frac{Q_0}{\rho c_p}(\vartheta - \vartheta_\infty) + \frac{Dk_\vartheta}{c_s c_p}\frac{\partial^2 \varphi}{\partial y^2} + \tau\left[D_B\frac{\partial \varphi}{\partial y}\frac{\partial \vartheta}{\partial y} + \frac{D_\varphi}{\vartheta_\infty}\left(\frac{\partial \vartheta}{\partial y}\right)^2\right] - \beta_i\left[u_2\frac{\partial u_2}{\partial x}\frac{\partial \vartheta}{\partial x} + u_3\frac{\partial u_3}{\partial y}\frac{\partial \vartheta}{\partial y} + u_2\frac{\partial u_3}{\partial x}\frac{\partial \vartheta}{\partial y} + u_3\frac{\partial u_2}{\partial y}\frac{\partial \vartheta}{\partial x}\right.$$

$$+2u_2u_3\frac{\partial^2\vartheta}{\partial x\partial y}+u_2^2\frac{\partial^2\vartheta}{\partial x^2}+u_3^2\frac{\partial^2\vartheta}{\partial y^2}\Bigg] \tag{31}$$

$$u_2\frac{\partial\varphi}{\partial x}+u_3\frac{\partial\varphi}{\partial y}=D(\vartheta)\frac{\partial^2\varphi}{\partial y^2}+D(\vartheta)\frac{\partial\varphi}{\partial x}\frac{\partial D(\vartheta)}{\partial y}-k_l(\varphi-\varphi_\infty)-\frac{\partial(V_\vartheta\varphi)}{\partial y}+\frac{Dk_\vartheta}{\vartheta_m}\frac{\partial^2\vartheta}{\partial y^2}+\frac{D_\vartheta}{\vartheta_\infty}\frac{\partial^2\vartheta}{\partial y^2}$$

$$-\beta_j\Bigg[u_2\frac{\partial u_2}{\partial x}\frac{\partial\varphi}{\partial x}+u_3\frac{\partial u_3}{\partial y}\frac{\partial\varphi}{\partial y}+u_2\frac{\partial u_3}{\partial x}\frac{\partial\varphi}{\partial y}+u_3\frac{\partial u_2}{\partial y}\frac{\partial\varphi}{\partial x}+2u_2u_3\frac{\partial^2\varphi}{\partial x\partial y}+u_2^2\frac{\partial^2\varphi}{\partial x^2}+u_3^2\frac{\partial^2\varphi}{\partial y^2}\Bigg] \tag{32}$$

$$u_2\frac{\partial N}{\partial x}+u_3\frac{\partial N}{\partial y}=D_n(\vartheta)\frac{\partial^2N}{\partial y^2}-\frac{bWc}{\Delta\varphi}\left[\frac{\partial N}{\partial y}\frac{\partial\varphi}{\partial y}+\frac{\partial^2\varphi}{\partial y^2}\right] \tag{33}$$

subject to the boundary conditions:

$$u_2=Bx\ ,u_3=-v(x)\ ,\varphi=\varphi_w\ ,\vartheta=\vartheta_w\quad ,at\ \ y=0 \tag{34}$$

$$u_2\longrightarrow 0\ ,\vartheta\longrightarrow\vartheta_\infty\ ,\varphi\longrightarrow\varphi_\infty\ ,as\ \ y\longrightarrow\infty \tag{35}$$

The transformed equations are:

$$\gamma\left(1+\frac{1}{\beta}\right)\left[f'''+\theta'f''-\theta f'''+\frac{1}{Po}\right]+\left(1+\frac{1}{\beta}\right)f'''+\alpha\left[ff^{iv}+2f'f'''+2(f'')^2\right]$$

$$-(f')^2-Mf'+ff''+Gr\theta+Gm\varphi+Gn\epsilon=0 \tag{36}$$

$$\left[(1+\gamma_2\theta)+\frac{4}{3}R\left(1+(\theta_3-1)\right)^3\right]\theta''-Prf\theta'+\delta(\theta')^2+PrEc\left[(1+\gamma\theta)(f')^2+\gamma(f')^2\theta'\right]$$

$$-Pr\Delta_x\theta+PrD_p\varphi''+Nb\varphi'\theta'+Nt(\theta')^2-\gamma_h(f'f'\theta'+ff^2\theta'')=0 \tag{37}$$

$$(1+\gamma_3\varphi)\varphi''+(1+\gamma_3\varphi)(\varphi')^2+Scf\varphi'-ScKr\varphi+Sc\tau[\theta'\varphi+\varphi\theta'']+ScSo\theta''-\gamma_0(ff'\varphi'+f^2\varphi'')=0 \tag{38}$$

$$(1+\gamma_4\epsilon)\epsilon''+(1+\gamma_4\epsilon)(\epsilon')^2+Lbf\epsilon'-LbPe\left(\epsilon'\varphi+\varphi''(\sigma+\epsilon)\right)=0 \tag{39}$$

together with the associated boundary conditions:

$$f'=1,\ f=S_w,\ \theta=1,\ \varphi=1,\ \epsilon=1,\ \ at\ \ \eta=0 \tag{40}$$

$$f'\longrightarrow 0,\ \theta\longrightarrow 0,\ \varphi\longrightarrow 0,\ \epsilon\longrightarrow 0,\ \ as\ \ \eta\longrightarrow\infty \tag{41}$$

The definition of pertinent flow parameters are as follows: $\alpha=\frac{k_0c}{\nu\rho}$ = viscoelastic parameter, $\gamma=b(\vartheta_w-\vartheta_\infty)$ = variable viscosity parameter, $Po=\frac{\rho ck}{\mu^*}$ = Porosity parameter $M=\frac{\sigma B_0^2}{\rho c}$ = Magnetic parameter, $G_r=\frac{g\beta_t(\vartheta_w-\vartheta_\infty)}{c^2x}$ = Thermal Grashof number, $Sc=\frac{\nu}{D}$ = Schmidt number $G_m=\frac{g\beta_c(\varphi_w-\varphi_\infty)}{c^2x}$ = Mass Grashof number, $Kr=\frac{k_l}{c}$ = chemical reaction parameter, $R=\frac{4\sigma_0\vartheta_\infty^3}{3k_ek^*}$ = Radiation term $\gamma_2=\xi(\vartheta_w-\vartheta_\infty)$ = variable thermal conductivity, $Pr=\frac{\nu\rho c_p}{k^*}$ = Prandtl number, $Ec=\frac{(cx)^2}{c_p(\vartheta_w-\vartheta_\infty)}$ = Eckert number $\delta=\frac{Q_0}{c\rho c_p}$ = heat generation parameter, $\gamma_h=\beta_ic$ = heat flux parameter, $D_p=\frac{DK_\vartheta(varphi_w-\varphi_\infty)}{c_sc_p\nu(\vartheta_w-\vartheta_\infty)}$ = Dufour number $N_b=\frac{\tau D_B(\varphi_w-\varphi_\infty)}{\nu}$ = Brownian motion parameter, $N_t=\frac{\tau D_\vartheta(\vartheta_w-\varphi_\infty)}{\vartheta_\infty\nu}$ = Thermophoresis parameter $L_b=\frac{\nu}{D_B}$ = Lewis number, $So=\frac{Dk_\vartheta(\vartheta_w-\vartheta_\infty)}{\vartheta_m\nu(\varphi_w-\varphi_\infty)}$ = Soret number $G_n=\frac{g\beta_n(N_w-N_\infty)}{c^2x}$ = Bioconvective Grashof number.$\gamma_0=\beta_jc$ = mass flux parameter The quantities of engineering interest such as local skin friction coefficient (C_f), local Sherwood number (Sh), local Nusselt number (Nh) and local density microorganism number (Mh) are defined as follows:

$$C_f=\frac{\tau_w}{\rho u_{2w}^2},\ Nu=\frac{q_w}{K(\vartheta)(\vartheta_w-\vartheta_\infty)},\ Sh=\frac{S_w}{D(\varphi)(\varphi_w-\varphi_\infty)},\ Mh=\frac{M_w}{D_n(\vartheta)(N_w-N_\infty)}$$

where

$$\tau_w=\left[\mu(\vartheta)\left(1+\frac{1}{\beta}\right)\frac{\partial u_2}{\partial y}|_{y=0}-K_0\left(u_3\frac{\partial^3u_2}{\partial y^3}+u_2\frac{\partial^3u_2}{\partial x\partial y^2}-3\frac{\partial u_2}{\partial x}\frac{\partial^2u_2}{\partial y^2}\right)|_{y=0}\right]$$

$$q_w=-K(\vartheta)\left(\frac{\partial\vartheta}{\partial y}|_{y=0}-\frac{16\sigma_s\vartheta_\infty^3}{3Ke}\left(\frac{\partial^2\vartheta}{\partial y^2}\right)|_{y=0}\right),\ S_w=D(\vartheta)\left(\frac{\partial\varphi}{\partial y}|_{y=0}\right),\ M_w=D_n(\vartheta)\left(\frac{\partial N}{\partial y}|_{y=0}\right)$$

4. Method of solution

The transformed ODEs have been solved numerically by utilizing SRM. The procedure of SRM is based basically on the use of the Gauss–Seidel relaxation approach. This approach is employed to linearize and decouple the nonlinearly coupled ODEs. The Chebyshev pseudospectral technique is further utilized to discretize the set of equations (Motsa [47]). After this, the current iteration was implemented on the linear terms while the previous iterations were implemented on the nonlinear terms. Applying the SRM to the transformed equations (38)–(41) subject to (42) and (43) to obtain:

$$\gamma_1\left(1+\frac{1}{\beta}\right)f'''_{r+1}+a_{0,1}f''_{r+1}+a_{1,r}f'''_{r+1}+\frac{\gamma_1}{Po}\left(1+\frac{1}{\beta}\right)f'_{r+1}+\left(1+\frac{1}{\beta}\right)f'''_{r+1}+a_{2,r}f^{iv}_{r+1}$$

$$+a_{3,r}f''_{r+1}+a_{4,r}+a_{5,r}-Mf'_{r+1}+a_{6,r}f''_{r+1}+a_{7,r}=0 \tag{42}$$

$$\theta''_{r+1}+b_{0,r}\theta''_{r+1}+\frac{4}{3}R\theta''_{r+1}+b_{1,r}\theta'_{r+1}+b_{2,r}+b_{3,r}+b_{6,r}\theta'_{r+1}+b_{7,r}\theta''_{r+1}$$

$$+b_{4,r}+PrQ_o\theta_{r+1}+b_{5,r}=0 \tag{43}$$

$$\varphi''_{r+1}+c_{0,r}\varphi''_{r+1}+c_{1,r}+c_{2,r}\varphi_{r+1}+c_{3,r}\varphi'_{r+1}-ScKr\varphi_{r+1}+c_{4,r}\varphi_{r+1}+c_{5,r}\varphi_{r+1}$$

$$c_{5,r}\varphi_{r+1}+c_{6,r}+c_{7,r}\varphi'_{r+1}+c_{8,r}\varphi''_{r+1}=0 \tag{44}$$

$$\epsilon''_{r+1}+d_{0,r}\epsilon''_{r+1}+d_{1,r}+d_{2,r}\epsilon_{r+1}+d_{3,r}\epsilon'_{r+1}+d_{4,r}\epsilon'_{r+1}+d_{5,r}+d_{6,r}\epsilon_{r+1}=0 \tag{45}$$

The coefficient parameters are defined as follows:

$$a_{0,r}=\gamma_1\left(1+\frac{1}{\beta}\right)\theta'_r,\ a_{1,r}=-\gamma_1\left(1+\frac{1}{\beta}\right)\theta_r,\ a_{2,r}=\alpha f_{r+1},\ a_{3,r}=2\alpha f'_r$$

$$a_{4,r}=2\alpha\left(f''_{r+1}\right)^2,\ a_{5,r}=-\left(f'_{r+1}\right)^2,\ a_{6,r}=f_r,\ a_{7,r}=Gr\theta_r+Gm\varphi_r+Gn\epsilon_r$$

$$b_{0,r}=\gamma_2\theta_{r+1},\ b_{1,r}-Prf_{r+1},\ b_{2,r}=\gamma_2\left(\theta'_r\right)^2,\ b_{3,r}=PrEc\left(1+\frac{1}{\beta}\right)\left(f''_r\right)^2$$

$$b_{4,r}=PrEc\gamma_1\left(1+\frac{1}{\beta}\right)\left(f''_r\right)^2,\ b_{5,r}=PrDo\varphi''_r,\ b_{6,r}=-\beta_1f_rf'_r,\ b_{7,r}=-\beta_1f_{r+1}^2$$

$$c_{0,r}=\gamma_3\varphi_{r+1},\ c_{1,r}=\left(\varphi'_{r+1}\right)^2,\ c_{2,r}=\gamma_3\left(\varphi'_r\right)^2,\ c_{3,r}=Scf_{r+1},\ c_{4,r}=Sc\tau\theta'_{r+1}$$

$$c_{5,r} = Sc\tau\theta''_{r+1},\ c_{6,r} = ScSo\theta''_{r+1},\ c_{7,r} = -\beta_2 f'_{r+1} f_r,$$
$$c_{8,r} = -\beta_2 f_r^2,\ d_{0,r} = \gamma_4 \epsilon_r$$

$$d_{1,r} = \left(\epsilon'_r\right)^2,\ d_{3,r} = Lbf_{r+1},\ d_{4,r} = -LbPe\varphi_{r+1},$$
$$d_{5,r} = -LbPe\sigma\varphi''_r,\ d_{6,r} = -LbPe\varphi''_{r+1}$$

$$\xi_j = cos\frac{\pi j}{N}, \quad j = 0, 1, 2, \ldots, N; \quad 1 \le \xi \le -1 \tag{46}$$

The domain of the analysis is $[0, \infty)$. This domain was changed to $[-1, 1]$ so as to implement the procedures of SRM. To change the domain, a mapping interval function is defined as:

$$\frac{\eta}{L} = \frac{\xi + 1}{2}, \quad -1 \le \xi \le 1 \tag{47}$$

The scaling function L was explored to solve for the problem boundary constraints at infinity. Therefore, an initial guess was chosen to conform with the problem boundary constraints. This is defined as follows:

$$f_0(\eta) = S_w - e^{-\eta},\ \theta_0(\eta) = e^{-\eta},\ \phi_0(\eta) = e^{-\eta},\ \ \epsilon_0(\eta) = e^{-\eta} \tag{48}$$

Hence, the problem in this paper is solved iteratively by starting from the initial guess defined in Eq. (48). To solve Eqs. (42)–(45), the finite difference and Chebyshev spectral collocation approaches were utilized to discretize the set of equations. The finite difference scheme is defined as centering in functions as follows:

$$\left(\frac{df}{d\eta}\right)^{n+\frac{1}{2}} = \frac{f_j^{n+1} - f_j^n}{\Delta\eta}, \quad \left(\frac{d\theta}{d\eta}\right)^{n+\frac{1}{2}} = \frac{\theta_j^{n+1} - \theta_j^n}{\Delta\eta},$$
$$\left(\frac{d\phi}{d\eta}\right)^{n+\frac{1}{2}} = \frac{\phi_j^{n+1} - \phi_j^n}{\Delta\eta}, \left(\frac{d\varphi}{d\eta}\right)^{n+\frac{1}{2}} = \frac{\varphi_j^{n+1} - \varphi_j^n}{\Delta\eta} \tag{49}$$

The matrix differentiation **D**

$$\frac{d^r f}{d\eta^r} = \sum_{k=0}^{N} D_{ik}^r u(\xi_k) = D^r f, \quad \frac{d^r \theta}{d\eta^r} = \sum_{k=0}^{N} D_{ik}^r \theta(\xi_k) = D^r \theta, \qquad i = 0, 1, \ldots N \tag{50}$$

$$\frac{d^r \phi}{d\eta^r} = \sum_{k=0}^{N} D_{ik}^r \phi(\xi_k) = D^r \phi, \quad \frac{d^r \varphi}{d\eta^r} = \sum_{k=0}^{N} D_{ik}^r \phi(\xi_k) = D^r \varphi, \qquad i = 0, 1, \ldots N \tag{51}$$

Simplifying the above Eqs. (42)–(45) by applying the Chebyshev differentiation matrix to obtain:

$$\left[\gamma_1\left(1 + \frac{1}{\beta}\right)D^3 + a_{0,r}D^2 + a_{1,r}D^3 + \frac{\gamma_1}{Po}\left(1 + \frac{1}{\beta}\right)D + \left(1 + \frac{1}{\beta}\right)D^3 + a_{2,r}D^4 + a_{3,r}D^3 - MD + a_{6,r}D^2\right] f_{r+1}$$

$$a_{4,r} + a_{5,r} + a_{7,r} = 0 \tag{52}$$

$$\left[D^2 + b_{0,r}D^2 + \frac{4}{3}RD^2 + b_{1,r}D + b_{6,r}D + b_{7,r}D^2 + PrQo\right]\theta_{r+1}$$

$$+b_{2,r} + b_{3,r} + b_{4,r} + b_{5,r} = 0 \tag{53}$$

$$\left[D^2 + c_{0,r}D^2 + c_{2,r} + c_{3,r}D - ScKr + c_{4,r} + c_{5,r} + c_{7,r}D + c_{8,r}D^2\right]\varphi_{r+1}$$

$$+c_{1,r} + c_{6,r} = 0 \tag{54}$$

$$\left[D^2 + d_{0,r}D^2 + d_{2,r} + d_{3,r}D + d_{4,r}D + d_{6,r}\right]\epsilon_{r+1} + d_{1,r} + d_{5,r} = 0 \tag{55}$$

Simplifying the above further by applying the implicit finite difference method we obtain Eqs. (56)–(59) (seeBox I).

The Eqs. (56)–(59) gives the following numerical scheme:

$$A_1 f_j^{n+1} = A_2 f_j^n - K_1 \tag{60}$$

$$B_1 \theta_j^{n+1} = B_2 \theta_j^n - K_2 \tag{61}$$

$$C_1 \varphi_j^{n+1} = C_2 \varphi_j^n - K_3 \tag{62}$$

$$D_1 \epsilon_j^{n+1} = B_2 \epsilon_j^n - K_4 \tag{63}$$

where the coefficient terms are defined by the equations in Box II.
The number used for collocation points in the numerical computation was N = 100 for all computations. The numerical simulations was done until a desired tolerance, say ϵ was reached. This tolerance level means the maximum values of infinity norm of difference between values of numerical computations.

5. Results and discussion

The transformed coupled fourth-order ODEs (36)–(39) subject to (40) and (41) were numerically solved using SRM in this study. The significance of changing controlled parameters on concentration ($\varphi(\eta)$), temperature ($\theta(\eta)$) and velocity $\left(\alpha\left(1 + \frac{1}{\beta}\right)f'(\eta)\right)$ has been presented in a pictorial manner. Fig. 1 represents the flow configuration of the antiviral mechanism of silver nanoparticles alongside the flow of Casson–Walters-B as a result of the holes in the vertical wall. The category of Casson fluid examined is honey, while polymethyl methacrylate is the Walters-B fluid examined. A mixture of these fluids within the BL is contaminated by viruses and bacteria. However, hybrid nanoparticles called silver nanoparticles serve as an agent to allow the growth of viruses and bacteria. The partition of the cytoplasm and nucleus in Fig. 1 explains the activity of the gelatinous liquid between the nucleus and the cell membrane. Fig. 2 depicts the geometrical configuration of the antibacterial mechanisms of silver nanoparticles alongside the BL dynamics of Casson–Walters-B fluids. The silver nanoparticles were observed to penetrate the regime where interaction between silver nanoparticles and the bacteria takes place. Based on this, disruption of intercellular molecules and adhesion to the bacterial membrane were noticed in Fig. 2. The cellular response is determined based on the nanomaterial size. Therefore, the antibacterial mechanism of AgNPs is influenced by their size and shape.

Fig. 3 represents the significance of varying viscosity on temperature and velocity. An increment in variable viscosity was detected to enhance the velocity figure. The Casson fluid (honey) as examined possesses antimicrobial properties as well as wound healing. The healing property of honey is because it offers antibacterial activity. It keeps a moist puncture condition and a higher viscosity assists in providing a protective hurdle to prevent infection. The activity of antibacterial in honey is a result of the enzymatic production of hydrogen peroxide. The wound-healing properties of honey are due to its antibacterial mechanism for moist wound conditions. Therefore, at high viscosity, the honey examined in this study served as a protective barrier to the prevention of infection. Fig. 4 shows the significance of thermal radiation on velocity along with temperature figures. An incremental value of the thermal radiation parameter was noticed to enhance the temperature and velocity figures. A nonlinear form of thermal radiation was considered in this study. It finds numerous applications in an environment where the temperature is very high. Fig. 4 shows that the heating of fluid particles is a mechanism to kill bacteria because of the drastic increase in thermal BL due to the increase in thermal radiation. Therefore, antimicrobial-resistant microorganisms occurred due to a higher value of the radiation parameter. The presence of Silver nanoparticles and high thermal radiation leads to the death of the viruses and bacteria within the boundary layer. Hence, the exposure of bacteria to polycations leads to cell membrane destruction.

$$\left(\frac{\gamma_1\left(1+\frac{1}{\beta}\right)D^3+a_{0,r}D^2+a_{1,r}D^3+\frac{\gamma_1}{Po}\left(1+\frac{1}{\beta}\right)D+\left(1+\frac{1}{\beta}\right)D^3+a_{2,r}D^4+a_{3,r}D^3-MD+a_{6,r}D^2}{2}\right)f_j^{n+1}$$
$$=-\left(\frac{\gamma_1\left(1+\frac{1}{\beta}\right)D^3+a_{0,r}D^2+a_{1,r}D^3+\frac{\gamma_1}{Po}\left(1+\frac{1}{\beta}\right)D+\left(1+\frac{1}{\beta}\right)D^3+a_{2,r}D^4+a_{3,r}D^3-MD+a_{6,r}D^2}{2}\right)f_j^{n}$$
$$-\left(a_{4,r}^{n+1}+a_{5,r}^{n+1}+a_{7,r}^{n+1}\right) \tag{56}$$

$$\left(\frac{D^2+b_{0,r}D^2+\frac{4}{3}RD^2+b_{1,r}D+b_{6,r}D+b_{7,r}D^2+PrQo}{2}\right)\theta_j^{n+1}$$
$$-=\left(\frac{D^2+b_{0,r}D^2+\frac{4}{3}RD^2+b_{1,r}D+b_{6,r}D+b_{7,r}D^2+PrQo}{2}\right)\theta_j^{n}$$
$$-\left(b_{2,r}^{n+1}+b_{3,r}^{n+1}+b_{4,r}^{n+1}+b_{5,r}^{n+1}\right) \tag{57}$$

$$\left(\frac{D^2+c_{0,r}D^2+c_{2,r}+c_{3,r}D-ScKr+c_{4,r}+c_{5,r}+c_{7,r}D+c_{8,r}D^2}{2}\right)\varphi_j^{n+1}$$
$$=-\left(\frac{D^2+c_{0,r}D^2+c_{2,r}+c_{3,r}D-ScKr+c_{4,r}+c_{5,r}+c_{7,r}D+c_{8,r}D^2}{2}\right)\varphi_j^{n}$$
$$-\left(c_{1,r}^{n+1}+c_{6,r}^{n+1}\right) \tag{58}$$

$$\left(\frac{D^2+d_{0,r}D^2+d_{2,r}+d_{3,r}D+d_{4,r}D+d_{6,r}}{2}\right)\epsilon_j^{n+1}$$
$$=-\left(\frac{D^2+d_{0,r}D^2+d_{2,r}+d_{3,r}D+d_{4,r}D+d_{6,r}}{2}\right)\epsilon_j^{n}-\left(d_{1,r}^{n+1}+d_{5,r}^{n+1}\right) \tag{59}$$

Box I.

Fig. 5 represents the significance of magnetics on the velocity figure. Magnetic therapy is a very good device for treating infectious diseases, pain, allergies, chronic wounds, and cancer. The imposed magnetic field to the non-Newtonian fluid flow has a frequency of about 100 Hz. It is good for water disinfection as well as non-thermal food preservation. Hence, the imposed magnetic field is observed in killing the microorganisms within the boundary layer by reducing the fluid velocity and the gyrotactic microorganisms. An incremental value of the magnetic parameter was noticed to lower the velocity of the fluid. This shows the magnetic slows down the motion of Casson–Walters-B fluids within the BL. This is due to the magnetic field producing Lorentz force which is capable of slowing down the dynamics of an electrically conducting fluid. The magnetic field as imposed to the mechanism of silver nanoparticles in the research increases the silver nanoparticles size due to an increasing laser energy. The laser energy is implemented in this research to boost the energy produced by the electromagnetic spectrum. Fig. 6 depicts the effect of the Prandtl number (Pr) on the velocity and temperature figures. The Pr controls the thermal conductivity of the silver nanoparticles and the fluids within the boundary layer. Physically, a small Pr increases the fluid temperature and hereby serves as an antimicrobial agent within the boundary layer. However, a higher Pr is noticed in Fig. 6 to lower the velocity and temperature of the fluid. This shows that, with increased Pr the viruses and bacteria can survive within the boundary layer. Fig. 7 illustrates the impact of Schmidt number (Sc) on the velocity along with concentration figures. The Sc explains the mass transfer of the fluids and the silver nanoparticles. Sc means dimensionless number which is the quotient of kinematic viscosity to mass diffusivity. Sc is employed to describe the mass diffusion convection of the silver nanoparticle mechanisms. An increment in Sc was detected to limit the velocity and concentration of Casson, Walters-B fluids, and silver nanoparticles.

The polymethyl methacrylate considered in this study is a synthetic resin that is derived from methyl methacrylate polymerization. Fig. 8 illustrates the impact of Walters-B fluid parameter (α) on the velocity figure. Physically, the variable viscosity along with thermal conductivity as explored in this study gives room for temperature changes which enhances the momentum BL thickness. Fig. 9 represents the impact of Casson parameter (β) on the velocity profile. The Casson fluid possesses a dynamic plastic viscosity which produces resistance to the Casson fluid flow phenomenon. The honey is the kind of Casson fluid examined in this analysis. Honey serves as an antimicrobial agent within the BL. This is evident in Fig. 9, as the Casson fluid parameter enhances the Gyrotactic microorganisms, viruses, and bacteria within the momentum boundary layer decreases. In the antiviral and antibacterial mechanisms, the silver nanoparticles penetrate the cells and bind with the cellular structures as well as biomolecules such as DNA, lipids, and proteins. This leads to the damage of the bacteria's internal structure. However, the silver nanoparticles serve as an antimicrobial agent to the bacteria and viruses on the non-Newtonian fluids considered in this research. In Fig. 10 and Fig. 11, the impact of varying heat flux

$$A_1 = \left(\frac{\gamma_1 \left(1+\frac{1}{\beta}\right) D^3 + a_{0,r} D^2 + a_{1,r} D^3 + \frac{\gamma_1}{Po}\left(1+\frac{1}{\beta}\right) D + \left(1+\frac{1}{\beta}\right) D^3 + a_{2,r} D^4 + a_{3,r} D^3 - M D + a_{6,r} D^2}{2} \right)$$

$$A_2 = -\left(\frac{\gamma_1 \left(1+\frac{1}{\beta}\right) D^3 + a_{0,r} D^2 + a_{1,r} D^3 + \frac{\gamma_1}{Po}\left(1+\frac{1}{\beta}\right) D + \left(1+\frac{1}{\beta}\right) D^3 + a_{2,r} D^4 + a_{3,r} D^3 - M D + a_{6,r} D^2}{2} \right)$$

$$B_1 = \left(\frac{D^2 + b_{0,r} D^2 + \frac{4}{3} R D^2 + b_{1,r} D + b_{6,r} D + b_{7,r} D^2 + PrQo}{2} \right)$$

$$B_2 = -\left(\frac{D^2 + b_{0,r} D^2 + \frac{4}{3} R D^2 + b_{1,r} D + b_{6,r} D + b_{7,r} D^2 + PrQo}{2} \right)$$

$$C_1 = \left(\frac{D^2 + c_{0,r} D^2 + c_{2,r} + c_{3,r} D - ScKr + c_{4,r} + c_{5,r} + c_{7,r} D + c_{8,r} D^2}{2} \right)$$

$$C_2 = -\left(\frac{D^2 + c_{0,r} D^2 + c_{2,r} + c_{3,r} D - ScKr + c_{4,r} + c_{5,r} + c_{7,r} D + c_{8,r} D^2}{2} \right)$$

$$D_1 = \left(\frac{D^2 + d_{0,r} D^2 + d_{2,r} + d_{3,r} D + d_{4,r} D + d_{6,r}}{2} \right)$$

$$D_2 = -\left(\frac{D^2 + d_{0,r} D^2 + d_{2,r} + d_{3,r} D + d_{4,r} D + d_{6,r}}{2} \right)$$

$$K_1 = \left(a_{4,r}^{n+1} + a_{5,r}^{n+1} + a_{7,r}^{n+1} \right), \; K_2 = \left(b_{2,r}^{n+1} + b_{3,r}^{n+1} + b_{4,r}^{n+1} + b_{5,r}^{n+1} \right)$$

$$K_3 = -\left(c_{1,r}^{n+1} + c_{6,r}^{n+1} \right), \; K_4 = \left(d_{1,r}^{n+1} + d_{5,r}^{n+1} \right)$$

Box II.

Table 1
Comparison of present study with Animasaun [48] when $\gamma_3 = \gamma_4 = \Delta_x = So = \alpha = 0$ and the absence of density microorganisms equations.

	Animasaun [48] $-\theta'(0)$	Present work $-\theta'(0)$
$\gamma_2 = 0$	1.81056406	1.18653737
$\gamma_2 = 2$	1.48607432	1.17522966
$\gamma_2 = 4$	1.07528692	1.17458078
$\gamma_2 = 6$	1.84218412	1.13768490

Table 2
Computational values of C_f, Nu, Sh, and Mh for pertinent flow parameters such as magnetic, Prandtl, Schmidt, thermal radiation, Walters-B and Casson fluid parameters.

M	Pr	Sc	R	α	β	C_f	Nu	Sh	Mh
0.5						1.793998	0.893098	0.499102	0.872140
1.0						1.542684	0.893098	0.499102	0.872140
1.5						0.844260	0.893098	0.499102	0.872140
	0.71					1.307347	0.803890	0.771249	0.821049
	1.2					1.069617	1.197030	0.771249	0.821049
	7.0					0.946103	1.591925	0.771249	0.821049
		0.22				1.246393	0.995821	1.137209	1.012469
		0.38				1.020628	0.995821	1.819645	1.012469
		0.61				0.908138	0.995821	2.497855	1.012469
			0.5			1.690696	0.554335	0.813301	0.942401
			1.0			1.795584	0.574592	0.813301	0.942401
			1.5			1.874743	0.629968	0.813301	0.942401
				0.4		1.432802	0.714240	0.914200	0.984120
				0.8		2.115686	0.714240	0.914200	1.840241
				1.2		2.798571	0.714240	0.914200	2.762141
					2.0	1.630620	0.436513	0.634102	1.456102
					4.0	1.828538	0.179316	0.634102	1.255200
					6.0	2.026456	0.077881	0.634102	0.942405

parameter and mass flux parameter are presented. It was observed that an increase in this parameters lead to an increase in velocity profile. However, the heat flux parameter increases the temperature profile while the mass flux parameter increases the fluid concentration. (see Fig. 10 and Fig. 11).

Table 1 shows the correctness of the present study when compared with the previous work of Animasaun [48]. Table 2 shows the significance of control parameters on the quantities of engineering interest. The computations show that magnetic field parameters can be used to control the simultaneous flow of Casson-Walters-B fluids. This is evident from Table 1 where an increase in magnetic parameter decreases the local skin friction and is negligible on Nu, Sh, and Mh. A higher value of Pr was noticed to degenerate the momentum boundary layer by decreasing the local skin friction. Due to the variable thermophysical parameters and a very high variable thermal conductivity, an increase in Pr was noticed to enhance the local Nusselt number and the entire thermal boundary layer. The impact of Walters-B (α) and Casson (β) fluids parameters are observed to simultaneously increase the local skin friction and the entire momentum BL respectively. Also, both α and β are found to greatly affect the local density of microorganisms. An increase in the thermal radiation parameter was observed in Table 1 to greatly enhance the momentum and thermal boundary layer by enhancing the local skin friction and local Nusselt number.

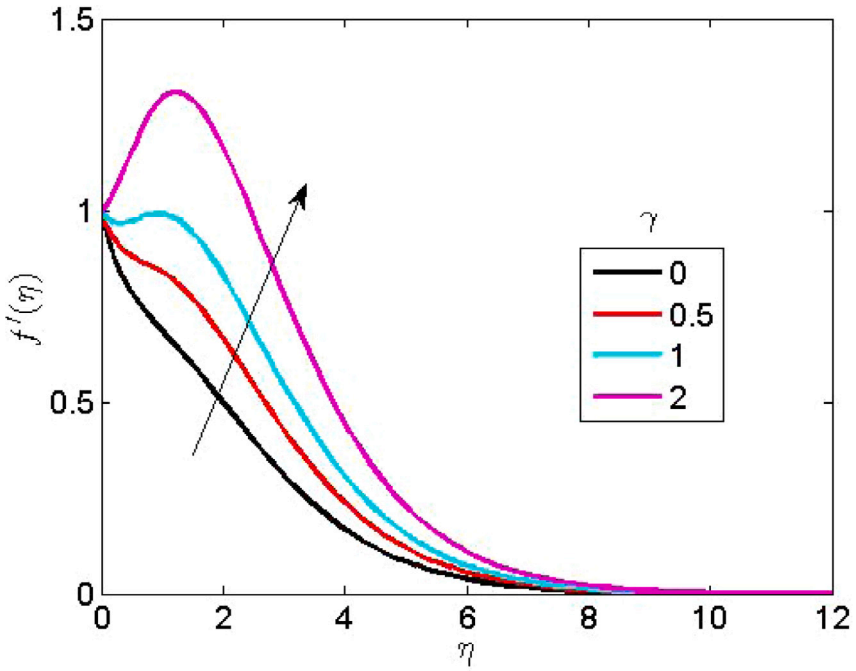

Fig. 3. Consequences of variable viscosity on the velocity figure.

6. Concluding remarks

This study gives a detailed analysis of the antiviral and antibacterial mechanisms of silver nanoparticles by considering the simultaneous flow of Casson and Walters-B with Gyrotactic microorganisms to the boundary layer. The transformed ODEs are solved using SRM. SRM is a technique that decouples and linearizes the coupled nonlinear ODEs. The MATLAB 2012 version was employed to implement the simulations. The numerical of collocation $N = 100$ while the dimensionless distance $\eta = 15$. The following are the key findings of this research:

1 The SRM was found accurate and converged faster as compared to studies in the literature.
2 Organic antibacterial materials are found to be less stable at a very high temperature. This is due to radiation along with heat generation within the BL.
3 The viruses as shown in Fig. 1 are smaller compared to the living cells. The virus is considered to be smaller than the bacterial.
4 The thermal radiation parameter is found to increase the fluid temperature. This increase in temperature figure in Fig. 4 resulted in the viral replication blockage as depicted in Fig. 1.
5 As the Casson along with Walters-B fluids enter through the vertical wall to the boundary layer, a reduction in their velocities was observed due to an increase in magnetic parameters.
6 Viruses as shown in Fig. 2 depend majorly on nuclear proteins before they can replicate.
7 By varying the viscosity along with thermal conductivity, the AgNPs, Casson, and Walters-B fluid are found to increase both velocities along the temperature figure as the Prandtl number increases.
8 In Fig. 2, AgNPs were found to penetrate the antibacterial regime and hereby disrupt the intercellular molecules due to an increase in Schmidt number. This shows that increasing the Schmidt number reduces the concentrations and the mechanisms of antiviral and antibacterial.

The findings of antiviral and antibacterial treatment as considered in this research find applications in dentistry, cancer treatment, drug delivery, DNA analysis, biosensors, catalysis, and magnetic resonance imaging (MRI). The synthesis process and design of silver nanoparticles as explored in this research as antibacterial properties of nanoparticles making cross-interpretation impossible in this study. Hence, the idea of silver nanoparticles as an antibacterial agents posed as a limitations to the study. The spectral relaxation method was utilized in this research because it helps in computing the problem derivatives at an infinite rate of convergence in space. Also, the chosen basis functions in solving the set of transformed equations are very flexible which leads to a very high accuracy as compared with other methods in literature.

CRediT authorship contribution statement

Ogiboina Ramakrishna: Writing of reviews & editing. **Bidemi Olumide Falodun:** Project Supervision & administration, methodology, investigation. **Oluwadamilare Joseph Akinremi:** Validation of results & funding acquisition. **Ezekiel Olaoluwa Omole:** Data curation. **Ahmed Senior Ismail:** Investigation, Writing of reviews & editing. **Femi Emmanuel Amoyedo:** Formal analysis, Conceptualization.

Declaration of competing interest

The authors declare that there is no conflict of interest.

Data availability

Data will be made available on request.

Acknowledgments

We appreciate the management of Landmark University, Omu-Aran, Nigeria for funding this article.

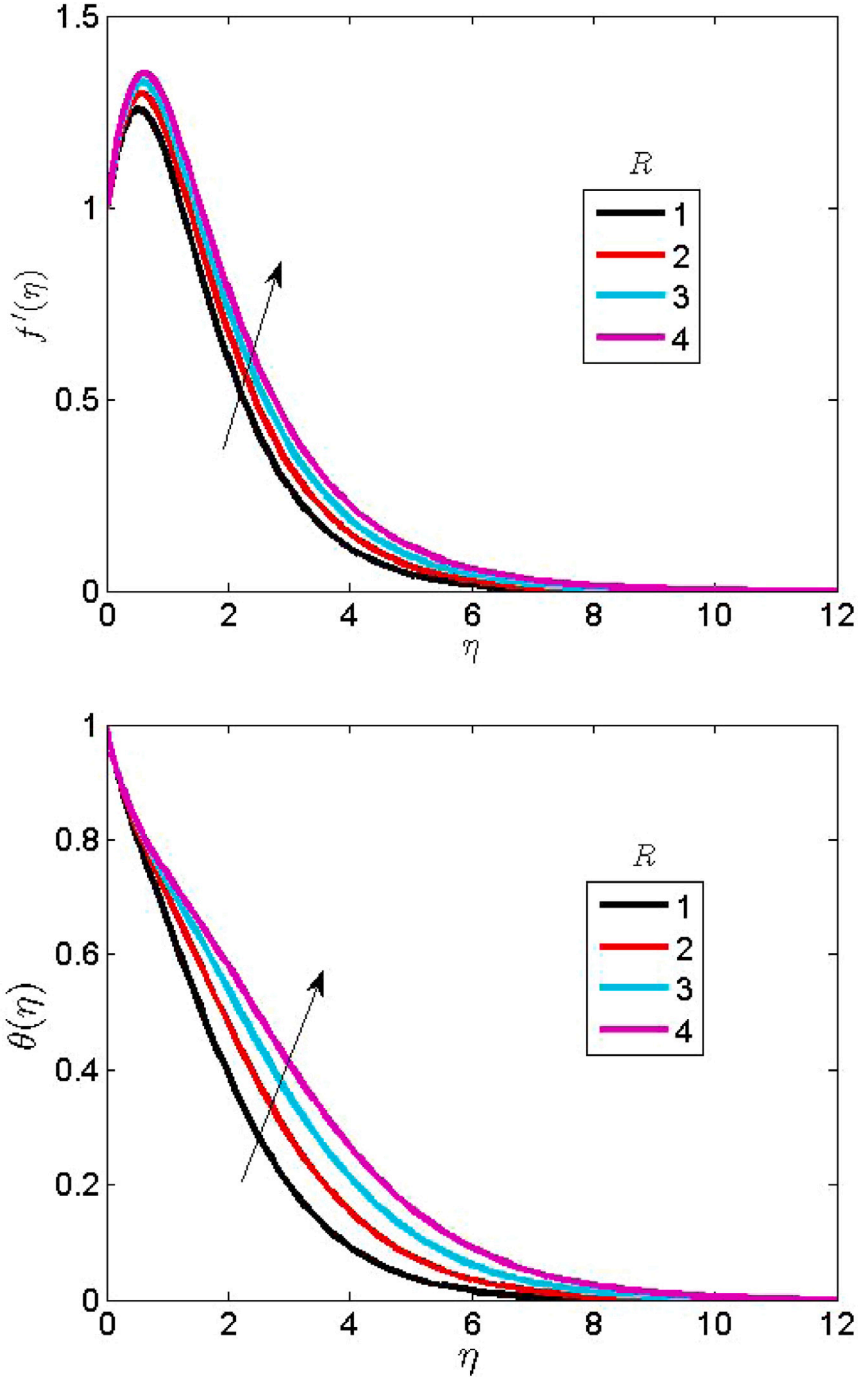

Fig. 4. Impact of thermal radiation on the velocity along with temperature figure.

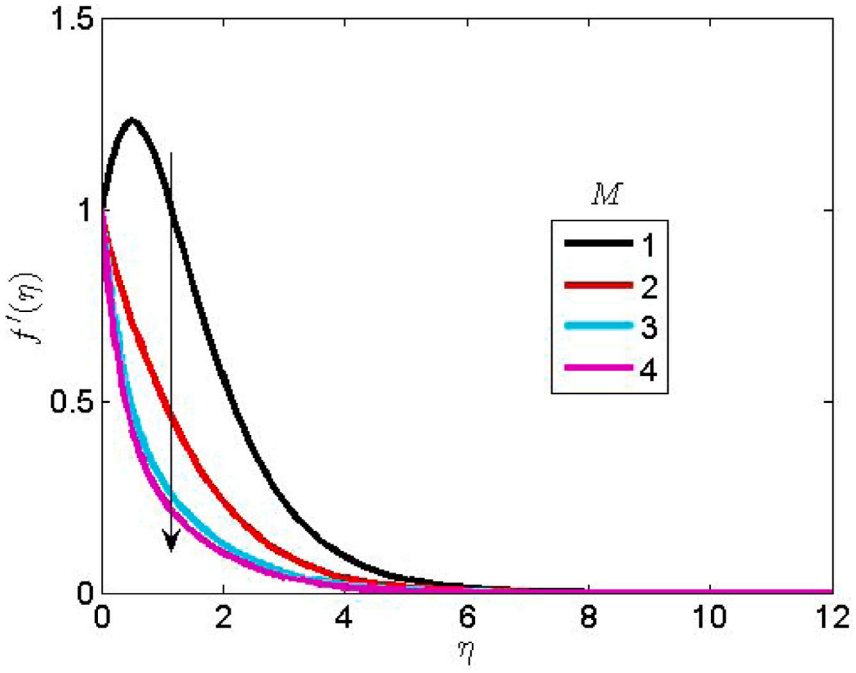

Fig. 5. Consequences of magnetic parameter on the velocity figure.

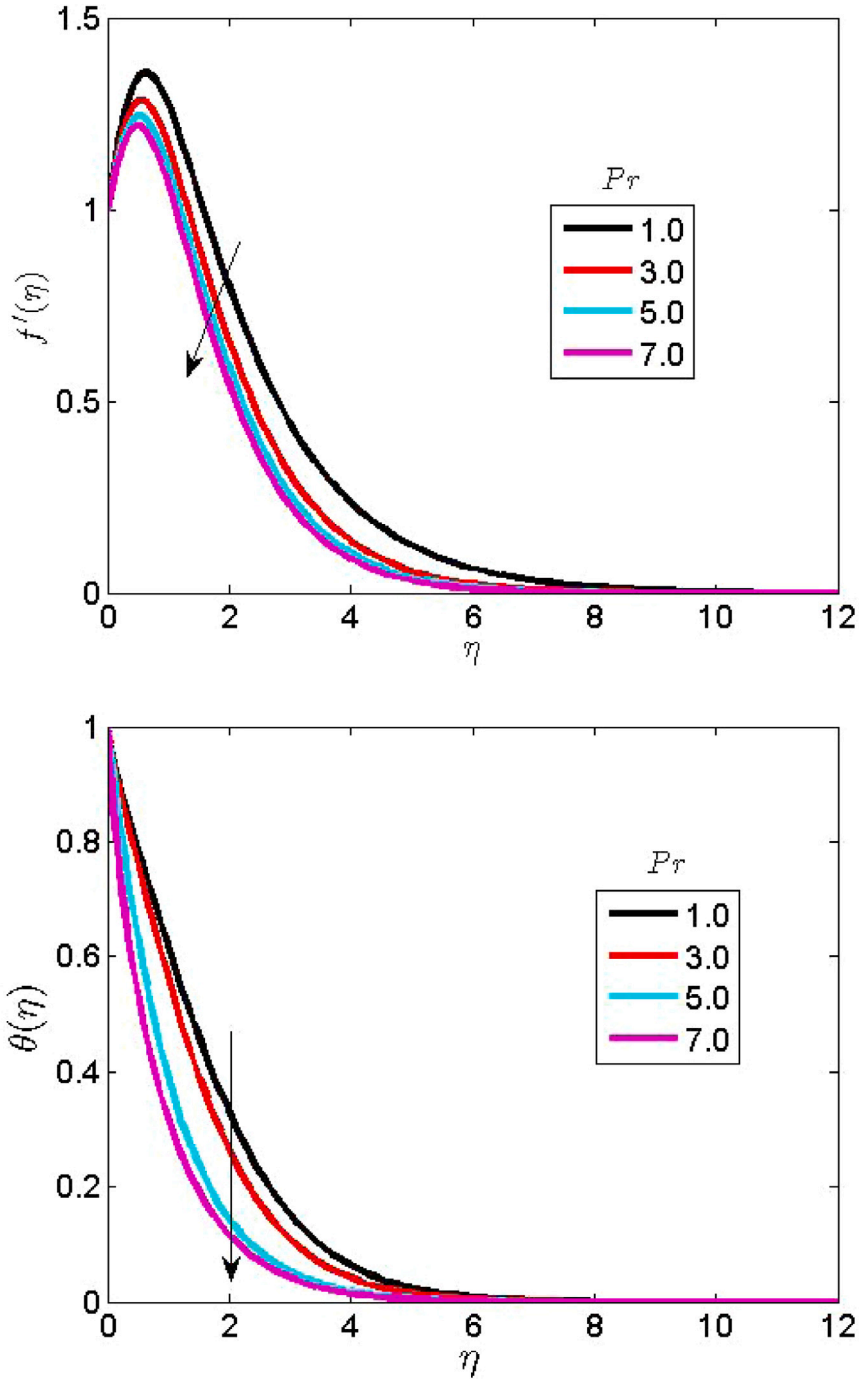

Fig. 6. Impact of Prandtl number on the velocity together with temperature figure.

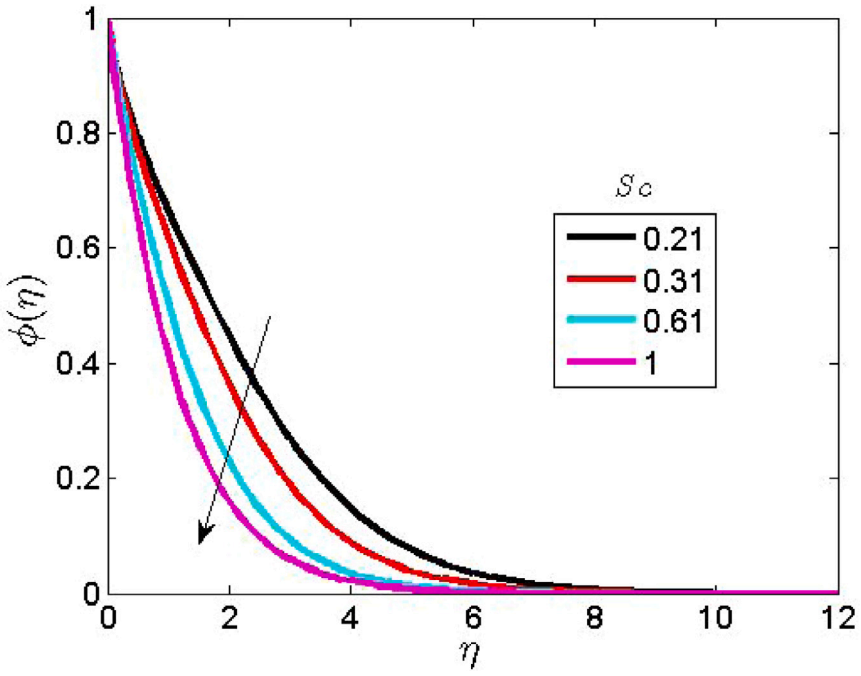

Fig. 7. Impact of Schmidt number on the velocity along with concentration figure.

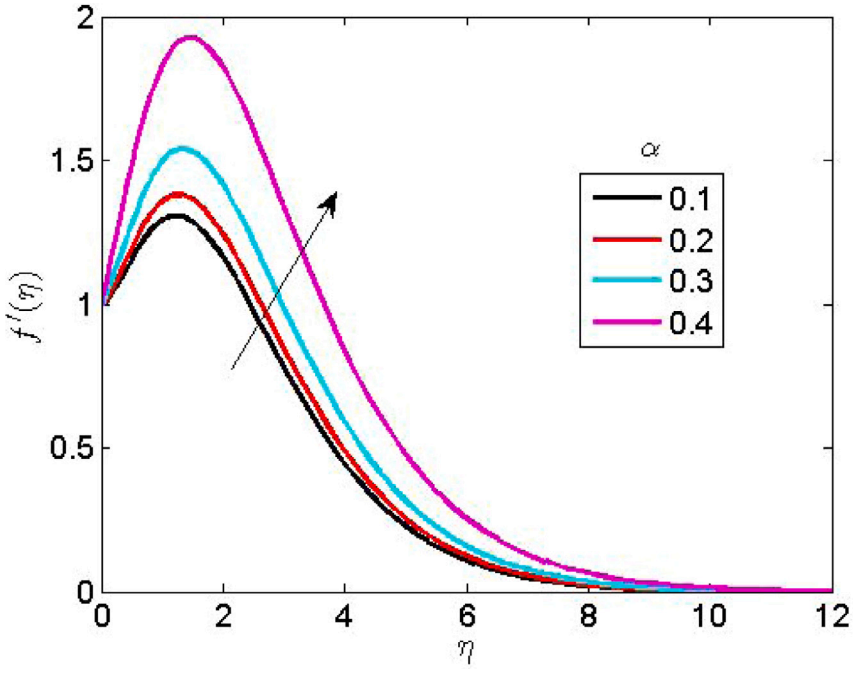

Fig. 8. Impact of Walters-B parameter on the velocity figure.

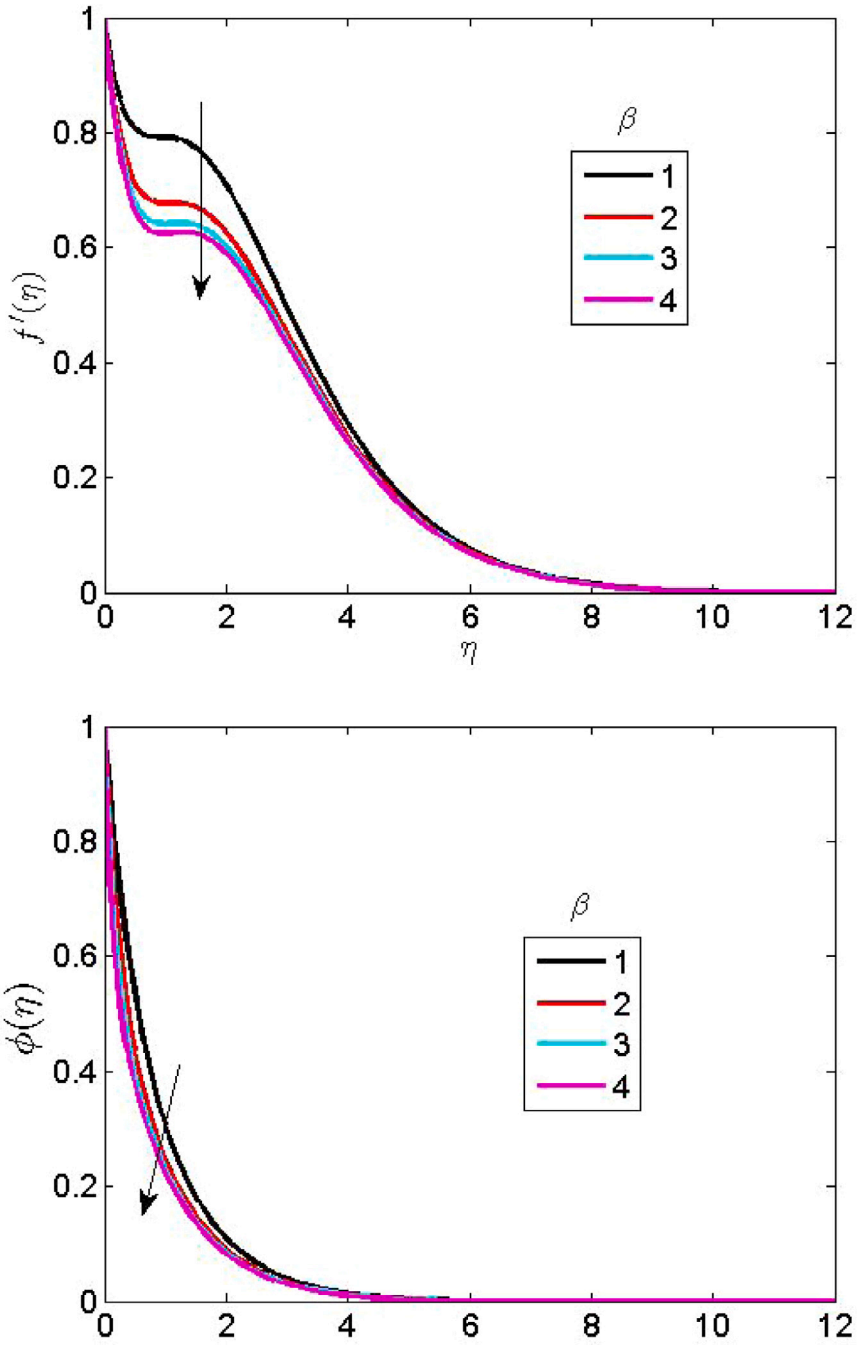

Fig. 9. Impact of Casson parameter on the velocity along with concentration figure.

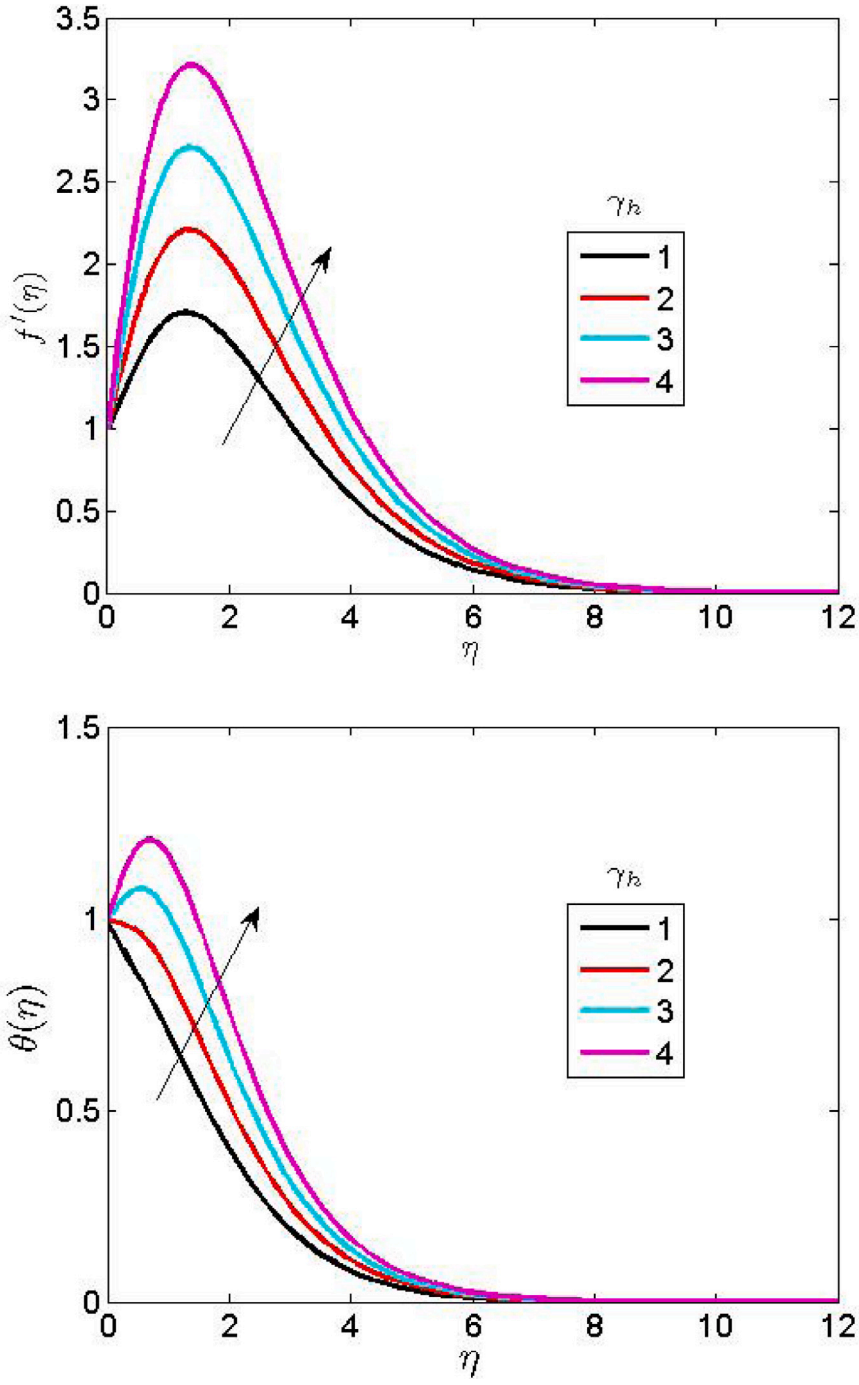

Fig. 10. Impact of heat flux parameter on the velocity along with temperature figure.

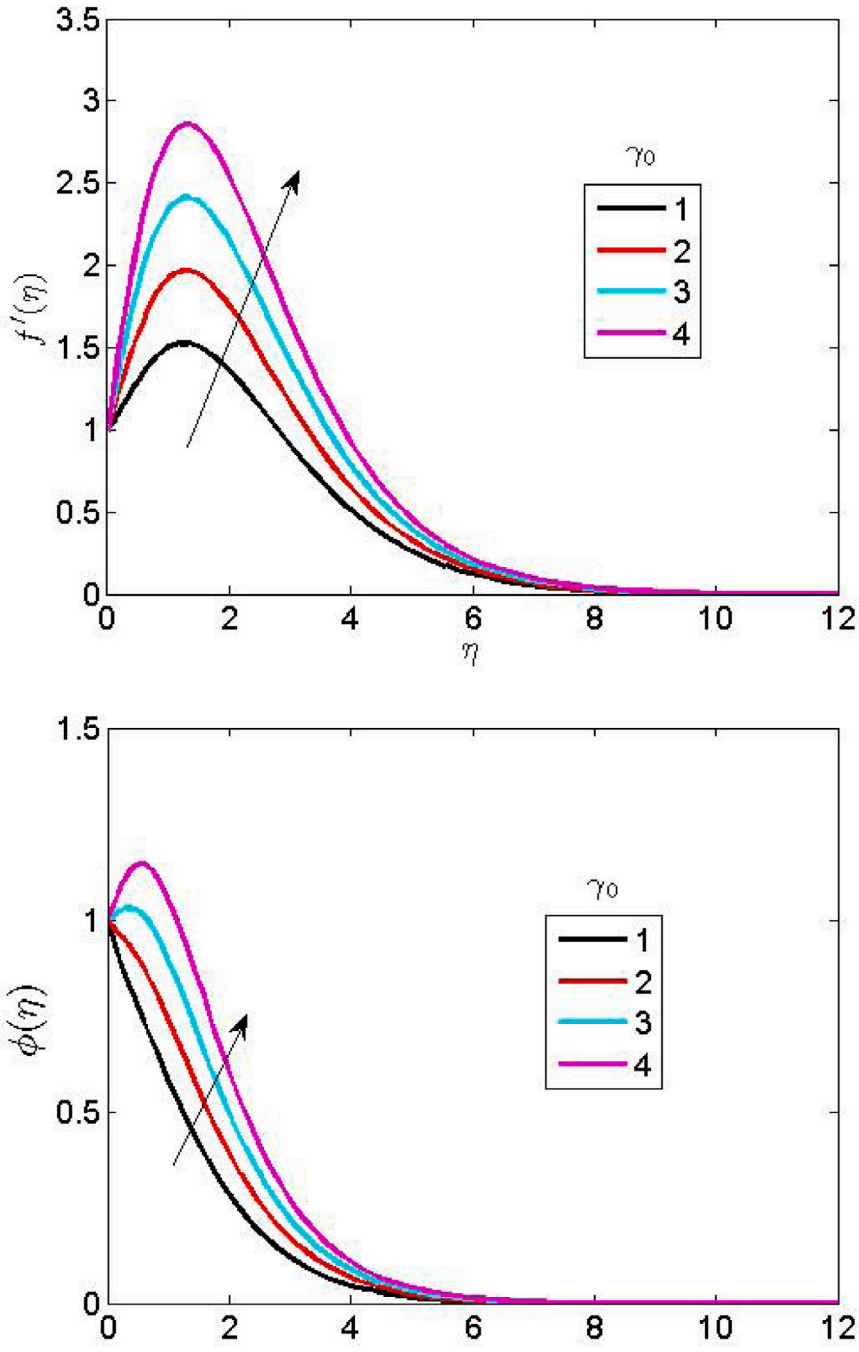

Fig. 11. Impact of mass flux on the velocity along with concentration figure.

References

[1] A. Gbadeyan Jacob, O. Akinremi Joseph, Entropy analysis of the nonlinear convective flow of a jeffrey fluid over an inclined sheet with variable electrical conductivity and thermal conductivity, Int. J. Eng. Res. Afr. (2021) http://dx.doi.org/10.4028/www.scientific.net/JERA.52.73.

[2] A.B. Vishalakshi, T. Maranna, U.S. Mahabaleshwar, D. Laroze, An effect of MHD on non-Newtonian fluid flow over a porous stretching/shrinking sheet with heat transfer, Appl. Sci. 12 (2022) 4937, http://dx.doi.org/10.3390/app12104937.

[3] A.S. Idowu, B.O. Falodun, Variable thermal conductivity and viscosity effects on non-Newtonian fluids flow through a vertical porous plate under Soret–Dufour influence, Math. Comput. Simulation 177 (2020) 358–384.

[4] E.A. Algehyne, S.A. Lone, Z. Raizah, S.M. Eldin, Saeed A, Galal AM, Mechanical characteristics of MHD of the non Newtonian magnetohydrodynamic Maxwell fluid flow past a bi-directional convectively heated surface with mass flux conditions, Front. Mater. 10 (2023) 1133133, http://dx.doi.org/10.3389/fmats.2023.1133133.

[5] K. Sudarmozhi, D. Iranian, Ilyas Khan, Amnah S.Al johani, Sayed M. Eldin, Magneto radiative and heat convective fow boundary layer in Maxwell fuid across a porous inclined vertical plate, Sci. Rep. 13 (2023) 6253, http://dx.doi.org/10.1038/s41598-023-33477-5.

[6] Soliman Hussein Abd Allah, Radiative MHD fow of Rivlin–Ericksen nanofuid of grade three through porous medium with uniform heat source, Beni-Suef Univ. J. Basic Appl. Sci. 11 (2022) 81.

[7] Raza Qadeer, Xiaodong Wang, Bagh Ali, Sayed M. Eldin, Huizhu Yang, Imran Siddique, Role of nanolayer on the dynamics of tri-hybrid nanofluid subject to gyrotactic microorganisms and nanoparticles morphology vis two porous disks, Case Stud. Therm. Eng. 51 (2023) 103534.

[8] Salah Yousef, Osama Al Mukbel, Yaman Sabsabi, S. Saranya, Qasem M. Al-Mdallal, Farzona Mukhamedova, Influence of PST and PHF heating conditions on the swirl flow of Al+Mg+TiO2 ternary hybrid water-ethylene glycol based nanofluid with a rotating cone, Int. J. Thermofluids 19 (2023) 100371.

[9] Sajjan Kiran, Nehad Ali Shah, N. Ameer Ahammad, C.S.K. Raju, M. Dinesh Kumar, Wajaree Weera, Nonlinear Boussinesq and Rosseland approximations on 3D flow in an interruption of ternary nanoparticles with various shapes of densities and conductivity properties, AIMS Math. 7 (10) 18416–18449, http://dx.doi.org/10.3934/math.20221014.

[10] M.R. Khan, N.A. Ahammad, S.E Alhazmi, A. Ali, M.A.H. Abdelmohimen, R. Allogmany, E. Tag-Eldin, MF. Yassen, Energy and mass transport through hybrid nanofluid flow passing over an extended cylinder with the magnetic dipole using a computational approach, Front. Energy Res. 10 (2022) 980042, http://dx.doi.org/10.3389/fenrg.2022.980042.

[11] Haq Izharul, Muhammad Bilal, N. Ameer Ahammad, Mohamed E. Ghoneim, Aatif Ali, Wajaree Weera*, Mixed convection nanofluid flow with heat source and chemical reaction over an inclined irregular surface, ACS Omega 7 (2022) 30477–30485.

[12] T. Gladys, G.R. Reddy, Contributions of variable viscosity and thermal conductivity on the dynamics of non-Newtonian nanofluids flow past an accelerating vertical plate, Partial Differ. Equ. Appl. Math. 5 (2022) 100264.

[13] V.R.R. Gurrampati, K. Vijaya, The buongiorno model with Brownian and thermophoretic diffusion for MHD casson nanofluid over an inclined porous surface, J. Nav. Archit. Mar. Eng. 19 (1) (2022) 31–45.

[14] Ahmad Sohail, Jihad Younis, Kashif Ali, Muhammad Rizwan, Muhammad Ashraf, Mohamed A. Abd El Salam, Impact of swimming gyrotactic microorganisms and viscous dissipation on nanoparticles flow through a permeable medium: A numerical assessment, J. Nanomater. 2022, 4888128, http://dx.doi.org/10.1155/2022/4888128, 11 pages.

[15] MM Bhatti, M Marin, A Zeeshan, R Ellahi, SI Abdelsalam, Swimming of motile gyrotactic microorganisms and nanoparticles in blood flow through anisotropically tapered arteries, Front. Phys. 8 (95) (2020) http://dx.doi.org/10.3389/fphy.2020.00095.

[16] Muhammad Faiz, Tahar Tayebi, Kashif Ali, Emad Hasani Malekshah, Sohail Ahmad, Interaction of nanoparticles with motile gyrotactic microorganisms in a Darcy-Forchheimer magnetohydrodynamic flow- A numerical study, Heliyon 9 (2023) e17840.

[17] Bhatti Muhammad Mubashir, Anwar Shahid, Tehseen Abbas, Sultan Z. Alamri, Rahmat Ellahi, Study of activation energy on the movement of gyrotactic microorganism in a magnetized nanofluids past a porous plate, Processes 8 (2020) 328, http://dx.doi.org/10.3390/pr8030328.

[18] Xu Yun Jie, Muhammad Bilal, Qasem Al Mdallal, Muhammad Altaf Khan, Taseer Muhammad, Gyrotactic micro organism fow of Maxwell nanofuid between two parallel plates, Sci. Rep. 11 (2021) 15142, http://dx.doi.org/10.1038/s41598-021-94543-4.

[19] Kada Belkacem, Iftikhar Hussain, Amjad Ali Pasha, Waqar Azeem Khan, Muhammad Tabrez, Khalid A. Juhany, Mostafa Bourchak, Ramzi Othman, Significance of gyrotactic microorganism and bioconvection analysis for radiative williamson fluid flow with ferromagnetic nanoparticles, Therm. Sci. Eng. Prog. 39 (2023) 101732.

[20] Chandra Priyanka, Raja Das, Impact of gyrotactic microorganisms in nanofluid via porous media along an inclined stretching plate: Finite element analysis, Numer. Heat Transfer B Int. J. Comput. Methodol. 83 (6) (2023) 367–394.

[21] Reddy Sudarsana Reddy, P. Sreedevi, Unsteady gyrotactic microorganisms and magnetic nanofluid heat and mass transfer analysis inside a chamber with thermal radiation, Int. J. Ambient Energy 45 (1) (2023) http://dx.doi.org/10.1080/01430750.2023.2277301.

[22] F.S. Hussain, N.Q. Abro, N. Ahmed, S.Q. Memon, N. Memon, Nano-antivirals: A comprehensive review, Front. Nanotechnol. 4 (2022) 1064615, http://dx.doi.org/10.3389/fnano.2022.1064615.

[23] D. Franco, G. Calabrese, S.P.P. Guglielmino, S. Conoci, Metal-based nanoparticles: Antibacterial mechanisms and biomedical application, Microorganisms 10 (2022) 1778, http://dx.doi.org/10.3390/microorganisms10091778.

[24] Salleh Atiqah, Ruth Naomi, Nike Dewi Utami, Abdul Wahab Mohammad, Ebrahim Mahmoudi, Norlaila Mustafa, Mh Busra Fauzi, The potential of silver nanoparticles for antiviral and antibacterial applications: A mechanism of action, Nanomaterials 10 (2020) 1566, http://dx.doi.org/10.3390/nano10081566.

[25] Soares Anna Rachel dos Santos, Loliza Luiz Figueiredo Houri Chalub, Rayssa Soares Barbosa, Deborah Egg de Paiva Campos, Allyson Nogueira Moreira, Raquel Conceiçao Ferreira, Prevalence and severity of non-carious cervical lesions and dentin hypersensitivity: association with oral-health related quality of life among Brazilian adults, Heliyon 7 (2021) e06492.

[26] Brandelli Adriano, The interaction of nanostructured antimicrobials with biological systems: Cellular uptake, trafficking and potential toxicity, Food Sci. Hum. Wellness 9 (2020) 8–20.

[27] Y.N. Slavin, J. Asnis, U.O. Häfeli, H. Bach, Metal nanoparticles: understanding the mechanisms behind antibacterial activity, J. Nanobiotechnol. 15 (1) (2017) 1–20.

[28] A.S. Idowu, B.O. Falodun, Soret–Dufour effects on MHD heat and mass transfer of Walter's-B viscoelastic fluid over a semi-infinite vertical plate: spectral relaxation analysis, J. Taibah Univ. Sci. 13 (1) (2019) 49–62, http://dx.doi.org/10.1080/16583655.2018.1523527.

[29] G. Gupta, P. Rana, Comparative study on Rosseland's heat flux on three-dimensional MHD stagnation-point multiple slip flow of ternary hybrid nanofluid over a stretchable rotating disk, Mathematics 10 (2022) 3342, http://dx.doi.org/10.3390/math10183342.

[30] Wang Fuzhang, Tanveer Sajid, Nek Muhammad Katbar, Wasim Jamshed, Mohamed R. Eid Usman, Assmaa Abd-Elmonem, Siti Suzilliana Putri Mohamed Isa, Sayed M. El Din, Computational examination of non-Darcian flow of radiative ternary hybridity Casson nanoliquid through moving rotary cone, J. Comput. Des. Eng. 10 (2023) 1657–1676.

[31] Rooman Muhammad, Anwar Saeed, Zahir Shah, Ahmed Alshehri, Saeed Islam, Poom Kumam, Panawan Suttiarporn, Electromagnetic trihybrid ellis nanofluid flow influenced with a magnetic dipole and chemical reaction across a vertical surface, ACS Omega 7 (2022) 36611–36622.

[32] Alhowaity Awatif, Muhammad Bilal, Haneen Hamam, M.M. Alqarni, Kanit Mukdasai, Aatif Ali, Non Fourier energy transmission in power law hybrid nanofuid fow over a moving sheet, Sci. Rep. 12 (2022) 10406, http://dx.doi.org/10.1038/s41598-022-14720-x.

[33] Qureshi Muhammad Amer, Irreversibility analysis of electromagnetic hybrid nanofuid for Cattaneo–Christov heat fux model using fnite element approach, Sci. Rep. 13 (2023) 4288, http://dx.doi.org/10.1038/s41598-023-31445-7.

[34] Ullah Zakir, Islam Zari, Taza Gul, Ishtiaq Ali, Wajdi Alghamdi, Fatima Ali, Darcy-Forchheimer hybrid nanofluids flow with quadratic convection over a stretched tube, Adv. Mech. Eng. 15 (6) (2023) 1–10.

[35] Adeyefa Emmanuel Oluseye, Ezekiel Olaoluwa Omole, Ali Shokri, Numerical solution of second-order nonlinear partial differential equations originating from physical phenomena using Hermite based block methods, Results Phys. 46 (2023) 106270.

[36] Fadugba Sunday Emmanuel, Shaalini Vinci, Joseph Temitayo Okunlola, Samuel Olukayode Ayinde1, Olanrewaju Femi, Development and analysis of a new third order method for solving initial value problems in ordinary differential equations, ABUAD J. Eng. Appl. Sci. (AJEAS) 1 (2) 137–142.

[37] Li Shuguang, A. Abbasi, W. Farooq, M. Gul, M. Ijaz Khan, Gulnoza Nafasova, Hala A. Hejazi, Heat and mass transfer characteristics of Al2O3/H2O and (Al2O3+Ag)/H2O nanofluids adjacent to a solid sphere: A theoretical study, Numer. Heat Transfer A (2024).

[38] S. Li, Safdar, M. Taj, M. Bilal, S. Ahmed, M. Ijaz Khan, Maimina Rafiq, Sherzod Shukhratovich Abdullaev, Generalized Lie similarity transformations for the unsteady flow and heat transfer under the influence of internal heating and thermal radiation, Pramana-J. Phys. 97 (2023) 203, http://dx.doi.org/10.1007/s12043-023-02672-4.

[39] Li Shuguang, M. Ijaz Khan, Sami Ullah Khan, Sherzod abdullaev, Habibullah, Montaha Mohamed Ibrahim Mohamed, M.S. Amjad, Effectiveness of melting phenomenon in two phase dusty carbon nanotubes (nanomaterials) flow of eyring-Powell fluid: Heat transfer analysis, Chinese J. Phys. 86 (2023) 160–169.

[40] Li Shuguang, Maria Imtiaz, M. Ijaz Khan, R. Naveen Kumar, Khafiza Samadovna Akramova, Applications of soret and dufour effects for Maxwell nanomaterial by convectively heated surface, Numer. Heat Transfer A (2024) http://dx.doi.org/10.1080/10407782.2024.14224.

[41] Tonekaboni Seyed Ali Madana, Ramin Abkar Reza Khoeilar, On the study of viscoelastic Walters'-B fluid in boundary layer flows, Math. Probl. Eng. 2012 (2017) 861508, http://dx.doi.org/10.1155/2012/861508, 1-18.

[42] A.G. Fredrickson, Principles and Applications of Rheology, Prentice-Hall Englewood Cliffs, NJ. USA, 1964.

[43] A. Mehmood, A. Ali, T. Shah, Heat transfer analysis of unsteady boundary layer flow by homotopy analysis method, Commun. Nonlinear Sci. Numer. Simul. 13 (5) (2008) 902–912.

[44] K. Walters, Non-Newtonian effects in some elastico-visocus liquids whose behavior at some states of shear is characterized by general equation of state, Quatum J. Mech. Appl. Maths 15 (1962) 63–73.

[45] F.I. Alao, A.I. Fagbade, B.O. Falodun, Effects of thermal radiation, Soret and Dufour on an unsteady heat and mass transfer flow of a chemically reacting fluid past a semi-infinite vertical plate with viscous dissipation, J. Nigerian Math. Soc. 35 (2016) 142158.

[46] A.I. Fagbade, B.O. Falodun, A.J. Omowaye, MHD natural convection flow of viscoelastic fluid over an accelerating permeable surface with thermal radiation and heat source or sink: Spectral homotopy analysis approach, Ain Shams Eng. J. 9 (2018) 10291041.

[47] S.S. Motsa, New iterative methods for solving nonlinear boundary value problems, in: Fifth Annual Workshop on Computational Applied Mathematics and Mathematical Modelling in Fluid Flow, in: School of Mathematics, Statistics and Computer Science, Pietermaritzburg Campus, 2012, pp. 9–13.

[48] I.L. Animasaun, Effects of thermophoresis, variable viscosity and thermal conductivity on free convective heat and mass transfer of non-Darcian MHD dissipative casson fluid flow with suction and nth order of chemical reaction, J. Nigerian Math. Soc. 34 (1) (2015) 11–31.